J. Earth Syst. Sci. (2023)132 151
https://doi.org/10.1007/s12040-023-02155-5

Geochemistry of the Bhor Saidan alluvial plains in Haryana state of north India: Implications for catchment weathering, provenance, and tectonic setting

Tarasha Chitkara[1,*], Anupam Sharma[2], O P Thakur[1] and N N Dogra[1]

[1]*Department of Geology, Kurukshetra University, Kurukshetra, Haryana, India.*
[2]*Birbal Sahni Institute of Palaeosciences, 53, University Road, Lucknow, Uttar Pradesh, India.*
**Corresponding author. e-mail: tarasha.chitkara@gmail.com*

MS received 5 August 2022; revised 16 May 2023; accepted 21 May 2023

The present study attempts to ascertain the sediment provenance of around 6.5-m thick palaeochannel sediment exposed in the vicinity of the Ghaggar–Hakra river system of the alluvial plains of the Haryana state of India. The major element geochemistry indicates that the sediments are arkosic in nature, dominated by quartz, K-feldspar, micas, plagioclase, and clay minerals (chlorite, illite, and a very less amount of montmorillonite). The CIA (chemical index of alteration) values ranged between 63 and 77, indicating moderate degrees of chemical weathering. REE plots show that the Eu anomaly is negative for average Bhor Saidan samples similar to PAAS and UCC, suggesting that they could have been deposited in the foreland basin after being originally produced from differentiated silicic and/or recycled sedimentary sources; nonetheless, a little positive Eu anomaly in the chondrite normalised plot is the result of feldspar and arkosic nature of sediments indicating higher levels of physical over the chemical weathering. Mostly the samples are from Siwaliks. Optically stimulated luminescence (OSL) dating suggests that the sediments are ∼11 ka old. Further, the palaeochannel is being incised ∼3.3 ka and younger sediments are stratigraphically deposited at lower levels. The discriminant function plots (Roser and Korsch 1988) of sediment samples exhibited that they were deposited in a passive margin setting and came from the interior of cratons or a quartzose sedimentary orogenic terrain. The present work done on the geochemistry of the sediments of a palaeochannel present in the alluvial plains will work as a dot on the map to connect the history of the river drainage system of the area in future studies.

Keywords. Quaternary; geochemistry; palaeochannel; alluvial plains; Bhor Saidan.

1. Introduction

The large alluvial plains (Indo-Gangetic plains) owe their evolution to the sediment generated and transported by the rivers originating from the Himalayan orogen. Aravalli–Delhi Ridge, which runs northeast to southwest, divides alluvial plains into two drainage basins (Singh 1996): the western alluvial plains (Punjab–Haryana) and the eastern alluvial plain (Ganga–Brahmaputra). A wide palaeochannel belt, the Ghaggar–Hakra channel is present in vast Indo-Gangetic Plains. This palaeochannel belt is deprived of the major drainage system, and it is mapped between the Ganga

Published online: 11 September 2023

and the Indus encompassing the east and west sides of the Indo-Gangetic Plains, respectively (Yashpal *et al.* 1980; Valdiya *et al.* 2005, 2013, 2016; Singh and Sinha 2019; Chaudhari *et al.* 2021). Saraswati is the mythological river of the Himalayas and is also believed to have existed in this northwestern part of vast alluvial plains and was flowing through the parts of Haryana, Punjab, Rajasthan, Gujrat, and modern Pakistan. In the last couple of decades, many types of research have been carried out in the Indo-Gangetic alluvial plains, and their relation with the Himalayas and our understanding of various aspects has been enhanced significantly; however, the existence of the Saraswati River and its course is still unresolved, due to the paucity of the subsurface geological data of the river's palaeocourse. Therefore, the workers are now taking more interest in this direction, and the work of Sinha *et al.* (2013), represented resistivity data along a buried palaeochannel of the Ghaggar River, wherein they inferred that there was a high energy wide braided river system which subsequently changed to a narrow channel seasonal river system. In a study, Singh *et al.* (1997) referred to two major tectonic phases, the older ∼40 ka and the other at ∼5–6 ka that caused the reorientation of several river systems. Recently, Singh *et al.* (2016) represented data from two drill cores from the buried palaeochannel of palaeo-Ghaggar. The study shows high-energy channel sand body deposit overlain by fine-grained, low-energy channel deposit, which is further overlain by reworked floodplain deposits. Based on the geochemical analysis, including the Rb–Sr isotopic composition, they established that sediments are derived largely from the higher Himalayas and once a well-established large river system existed in the region. The studied palaeochannel may be the palaeochannel of the Saraswati River (Chaudhari *et al.* 2021). In some relatively recent studies of buried palaeochannel of the Ghaggar River (Sinha *et al.* 2013; Singh *et al.* 2016), it has been inferred that the fluvial system setting changed from high energy wide network of braiding rivers to an incised river channel system and ultimately transformed into an ephemeral river system with small channels due to dwindling climatic conditions. The role of tectonics, however, coupled with climate may also have been invoked in some earlier studies (Singh and Sinha 2019).

The geochemical composition of siliciclastic sediments provides credible information on geological earth processes such as weathering and sediment transport, provenance, tectonic setting, etc. (Bhatia 1983; McLennan and Taylor 1983; Taylor and McLennan 1985; Wronkiewicz and Condie 1987; Cullers 1988; Feng and Kerrich 1990; Condie *et al.* 1992; McLennan *et al.* 1993; Garver and Scott 1995; Fedo *et al.* 1996; Nesbitt *et al.* 1996; McCann 1998; Singh and Rajamani 2001a, b; Tripathi *et al.* 2004; Singh 2009). The present study would provide insight into the provenance, weathering, and tectonic setting of the palaeochannel.

2. Study area

The study area lies ∼13 km west of Kurukshetra (between Pehowa and Bhor–Saidan villages, 29.965313N; 76.699775E) (figures 1 and 2). It is bordered in the north by the Himalayan foothills, in the east by the Yamuna River, in the west by the huge Thar Desert, and in the south by degraded Aravalli Hills. Markanda and Ghaggar rivers flow towards the southwest (western alluvial plain), whereas Yamuna River flows towards the east (Indo-Gangetic alluvial plain) (figure 3). The climate is semi-arid with mean annual precipitation of around 450 mm most of which is received during the Indian Summer Monsoon (ISM). The study area experiences maximum and minimum temperatures of 45 degrees and 2 degrees Celsius, respectively. Vegetation is dominated by tropical dry deciduous in the northeastern region; the Siwaliks region is covered by tropical moist deciduous and the western region has tropical thorn forests.

3. Methodology

The 6.5-m thick exposed sedimentary section of a palaeochannel was systematically sampled. A trench was made to collect samples, leaving the uppermost 0.6 m to minimise anthropogenic and surface contamination. A total of 62 samples were collected at 10 cm for sand-dominated horizons and 5 cm for clay-rich layers, out of which 36 representative samples were selected based on textural variations for geochemical analysis.

3.1 *Textural analyses*

Grain size analyses were carried out using a laser particle size analyser (Beckman-Coulter LS 13 320). For which, 10 g of sample was treated with different chemical reagents such as sodium acetate

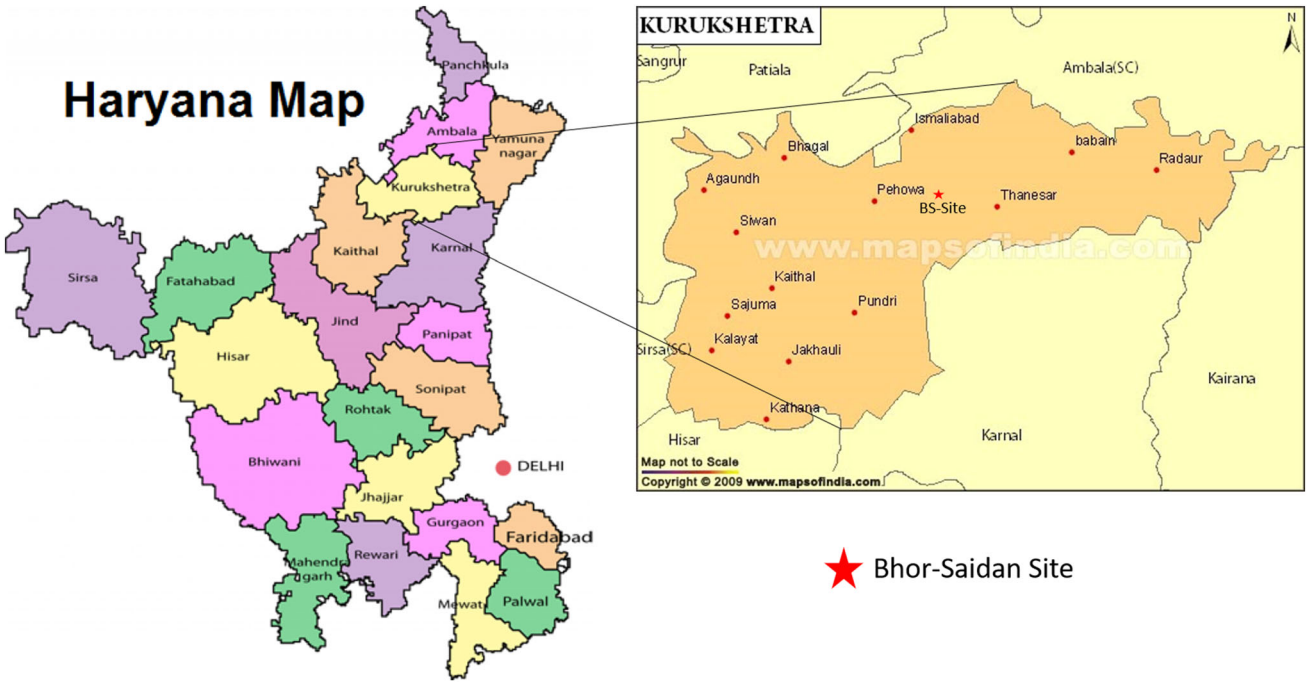

Figure 1. Map of India showing Haryana state, with further elaboration of the study area.

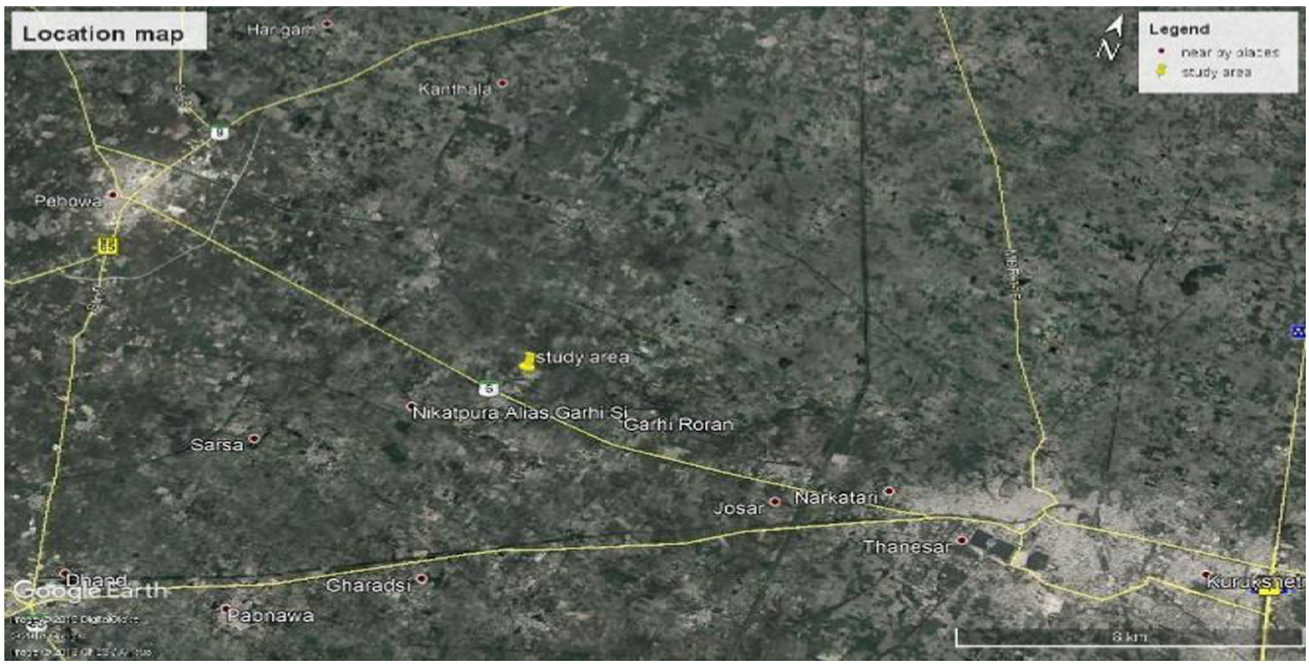

Figure 2. Google Earth map showing the location of the study area, yellow lines on the map are the state highways connecting the study area.

(1 N), hydrogen peroxide (30%), sodium citrate (0.3 M), and sodium dithionite combination to remove, carbonate, organic carbon, and iron-manganese coatings, respectively (Jackson 1956; Kunze and Dixon 1986). Finally, 1–2 ml of the well-homogenised samples were analysed in the laser particle size analyser.

3.2 *Mineralogical and geochemical analyses*

X-ray diffraction (XRD) analysis was done on well-crushed and homogenised powdered samples. The size and weight of the samples are <63 μm and 1–2 g, respectively. PANalytical Xpert3 instrument was used to find out the bulk mineralogical

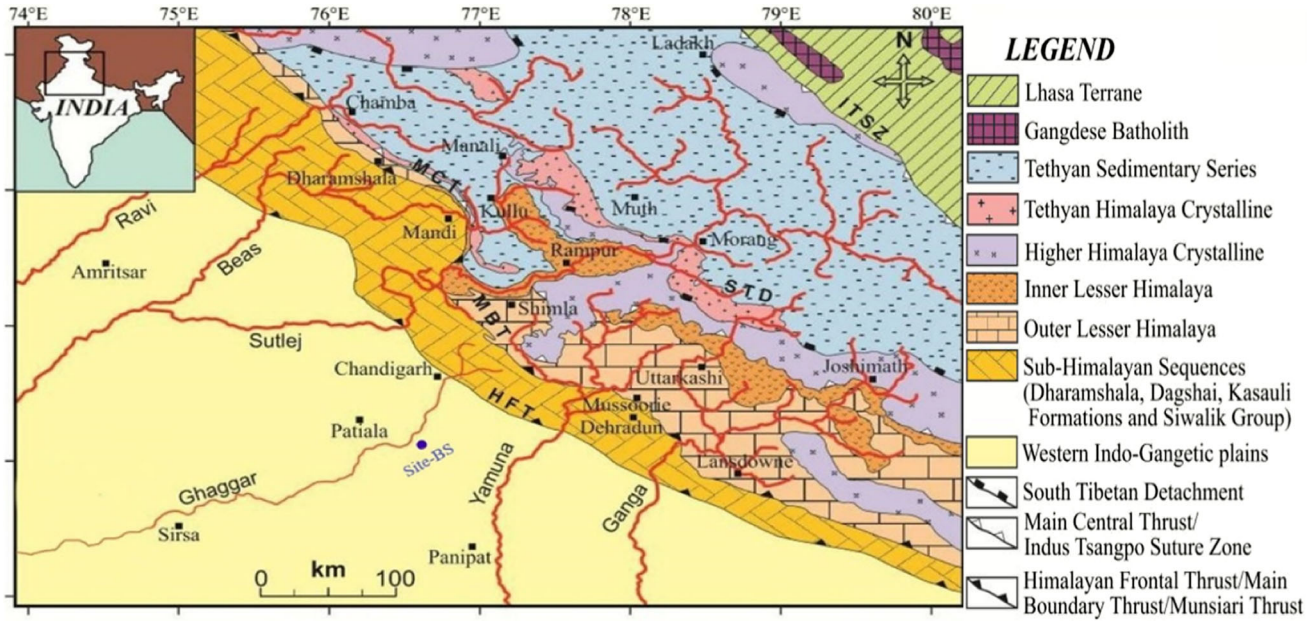

Figure 3. Simplified geological map of NW Himalaya along with major drainage and site location BS. The map is taken from Singh *et al.* (2016), based on the compilations taken from Webb *et al.* (2011), Yin (2006), Vannay *et al.* (2004), and Myrow *et al.* (2015).

distribution. A homogenised powdered sample with a mesh size of around 200 microns was utilised for the analysis of the major elements. To make the palettes, a 6:4 ratio of sample to boric acid was compacted (2500 psi) using a Kameyo Powder-Press. Using a wavelength-dispersive X-ray fluorescence spectrometer, the pellets were examined (WD-XRF; PANalytical AXios mAX). In this technique, a programme for computers that uses the matrix calibration method transformed X-ray counts into concentrations (Franzini *et al.* 1972). For major oxides, the analytical precision was 5%, while the accuracy ranged from 2 to 10%.

ICP-MS (Agilent 7700) is used to examine trace elements, together with rare earth elements (REE). Milli-Q ultra-pure (18.2 MΩ-cm) water was used to make a solution. All the samples were digested by taking 30 mg (–200 mesh) sediment powder by using supra pure acids (HF, $HCLO_4$, HNO_3). Four solutions (10, 50, 100, 200, and 300 ppb for all elements) were prepared by 71A and 71B multi-element calibration standard solutions (Inorganic Ventures make) for the external calibration of the machine. Two USGS rock powder standards, namely the Green River Shale (SGR-1b) and the Cody Shale (SCo-1), were used for analyses. All the datasets were well below from 5% error with a good calibration curve. The geochemical analyses were carried out at Birbal Sahani Institute of Palaeosciences, Lucknow.

3.3 *Optically stimulated luminescence (OSL) dating*

The date of the sedimentary succession of the palaeochannel was established using an optically stimulated luminescence (OSL) dating technique since the sediments contain less organic material (Aitken 1998; Wallinnga 2002). OSL dating is a widely used method to determine the age of river deposits by estimating the time since the last time they were exposed to sunlight (Duller 1996; Jain *et al.* 2004; Cordier *et al.* 2010; Morthekai and Ali 2014). The OSL samples were collected from the scraped section along with the sediment samples. Samples were opened in the OSL lab under low-intensity red lighting. To determine the water content and dosing rate, the pipe's first 3 cm sediment sample was taken out and preserved. The sediment samples were processed with 1N HCl to remove carbonates and 30% H_2O_2 to remove organic debris to extract the quartz. The samples were then dried in an oven at 45°C after being cleaned with distilled water. The dried samples were sieved to get grains that were 90–150 μm in size. Heavy minerals and feldspar were removed from the quartz fraction using an isodynamic separator set at 0.5 A and 1.5 A (Porat 2006). To remove the outer alpha skin (∼20 μm) and remaining feldspar, the cleaned quartz portion was scraped with 40% HF for 80 min. The samples were then cleaned of fluorides by being exposed to 12 N

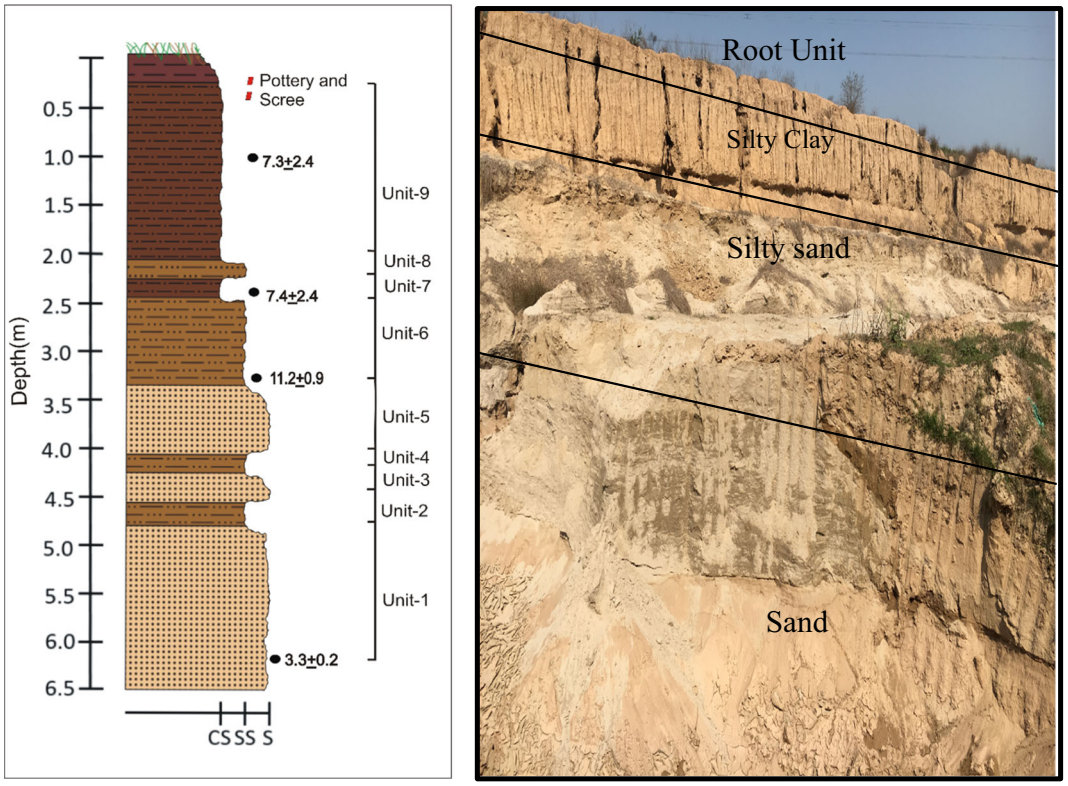

Figure 4. Field photograph of the Bhor Saidan Palaeochannel section showing different terraces and the litholog with details of texture and sedimentary structure. Sample locations are represented as solid dots outside litholog (bottom to top).

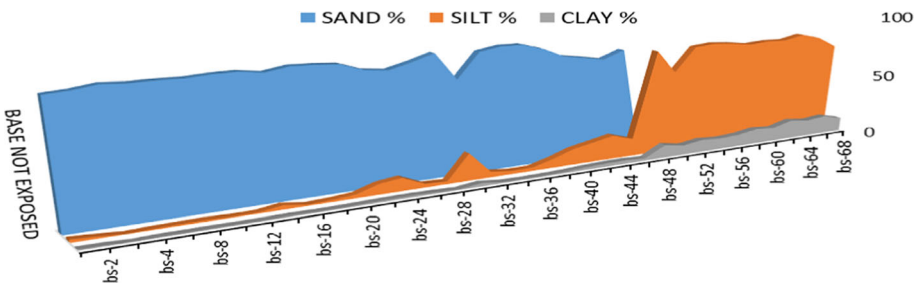

Figure 5. Depth-wise distribution of the grain size data of the lithology present in the area. This figure shows the number of samples and percentage of the grain size distribution (sand, silt and clay) from bottom to top of the section. Silt and clay dominate the upper part of the section.

HCl for 30 minutes. For measurements, an automated Risø TL-OSL reader (TL/OSL-DA-20) (Bøtter-Jensen *et al.* 2010) is used. An on-plate $^{90}Sr/^{90}Y$ beta source with a dosage rate of 5.96 Gy/min was used to irradiate the samples. To calculate the annual dose, the conversion factor suggested by Adamiec and Aitken (1998) was used to assess the radioactive material concentrations. A highly pure germanium detector (HPGe) was used to measure the U, Th, and K concentrations. To achieve radioactive equilibrium, the samples are stored for 21 days after being enclosed in plastic boxes. Determination of the cosmic rays to the dosage rate is calculated using the average water content of 5–10% and the Prescott and Hutton (1994) technique. Four samples were collected to establish the chronology.

4. Result

4.1 *Alluvial stratigraphy*

The sediments are dominated by grey and micaceous sand and silt facies with current bedding, ripple marks, and planar laminations, and are marked as Markanda Formation (Younger Alluvium) in the lithostratigraphic column. Further,

Table 1. *Textural analysis data of the sediments.*

Sample no.	Sand	Silt	Clay	Mean	Sorting	Skewness	Kurtosis	Median
bs-68	18.20	70.80	11.00	6.108	2.215	0.041	0.986	6.151
bs-66	5.70	79.50	14.80	6.949	1.946	0.067	1.093	6.895
bs-64	3.70	83.80	13.20	6.813	1.809	0.191	1.092	6.636
bs-62	4.00	80.80	15.20	6.981	1.872	0.148	1.160	6.818
bs-60	7.20	81.60	11.00	6.346	1.910	0.217	1.115	6.149
bs-58	6.80	80.80	12.40	6.558	1.947	0.155	1.022	6.409
bs-56	6.90	83.30	9.80	6.256	1.820	0.237	1.153	6.051
bs-54	6.60	84.80	9.00	6.216	1.758	0.227	1.164	6.032
bs-52	6.00	83.60	10.20	6.379	1.843	0.204	1.111	6.216
bs-50	17.20	65.00	7.90	5.667	1.939	0.291	1.075	5.371
bs-48	5.60	83.80	10.70	6.490	1.823	0.192	1.196	6.326
bs-46	83.60	14.20	2.10	2.743	1.429	0.478	1.684	2.464
bs-44	77.80	19.40	2.80	3.058	1.719	0.555	1.491	2.564
bs-42	81.00	16.00	2.70	2.779	1.799	0.598	2.321	2.185
bs-40	83.90	13.00	2.10	2.711	1.380	0.479	2.213	2.448
bs-38	91.50	7.30	1.20	2.598	0.930	0.282	1.444	2.520
bs-36	96.50	2.70	0.80	2.054	0.568	0.144	1.325	2.036
bs-34	97.00	2.60	0.60	1.855	0.755	0.017	1.323	1.892
bs-32	94.40	4.70	0.90	2.230	0.832	0.098	1.106	2.296
bs-30	75.30	21.90	2.70	3.302	1.602	0.521	1.484	2.879
bs-28	97.00	2.30	0.60	2.125	0.688	−0.043	1.380	2.141
bs-26	92.10	3.00	1.10	2.568	0.848	0.222	1.570	2.499
bs-24	88.10	10.50	1.40	2.727	1.100	0.304	1.861	2.619
bs-22	90.20	8.40	1.30	2.712	0.917	0.305	1.693	2.624
bs-20	96.20	2.90	1.00	2.669	0.530	0.098	1.168	2.654
bs-18	97.70	1.60	0.70	2.327	0.514	0.016	1.122	2.369
bs-16	98.40	0.90	0.60	2.165	0.483	0.014	1.063	2.154
bs-14	95.90	3.30	0.90	2.306	0.617	0.194	1.315	2.269
bs-12	98.50	0.80	0.60	1.868	0.446	0.034	1.033	1.862
bs-10	98.50	0.80	0.60	2.102	0.416	0.015	0.011	2.100
bs-8	97.70	1.30	0.70	2.120	0.452	−0.029	1.097	2.122
bs-6	98.40	1.10	0.60	2.142	0.403	0.035	1.022	2.137
bs-4	98.50	0.80	0.60	2.140	0.424	0.008	1.035	2.140
bs-3	99.80	0.20	0.00	2.088	0.387	−0.013	0.927	2.090
bs-2	97.70	1.50	0.70	2.039	0.489	−0.034	1.127	2.047
bs-1	96.80	2.50	0.80	2.060	0.496	0.017	1.187	2.063

Table 2. *OSL dating results of the sediment samples.*

Sample	U (ppm)	Th (ppm)	K (%)	De (Gy)	Dose rate (Gy ka^{-1})	Age (ka)
bs-42	1.1±0.4	15.9±12.7	0.6±0.1	13.6±0.8	1.8±0.6	7.4±2.4
bs-1	2.1±0.8	11.6±0.7	1.4±0.1	8.2±0.1	2.5±0.2	3.3±0.2
bs-60	4.0±1.0	13.5±2.3	1.6±0.1	23.6±1.4	3.2±0.2	7.3±0.7
bs-37	2.4±0.6	7.5±1.8	0.9±0.0	20.9±0.8	1.9±0.1	11.2±0.9

silty sand layers are intercalated with sand layers showing fluvial cycle influence in the palaeoriver channel (Thussu 1995). Based on the sediment texture and structures, the 6.5-m thick alluvial sequence is divided into nine units (figure 4). Stratigraphically, the base is not exposed. Unit 1 of the section is 1.6-m thick and is dominated by finer sand particles (96–98%) with only 2–3% of silt-size

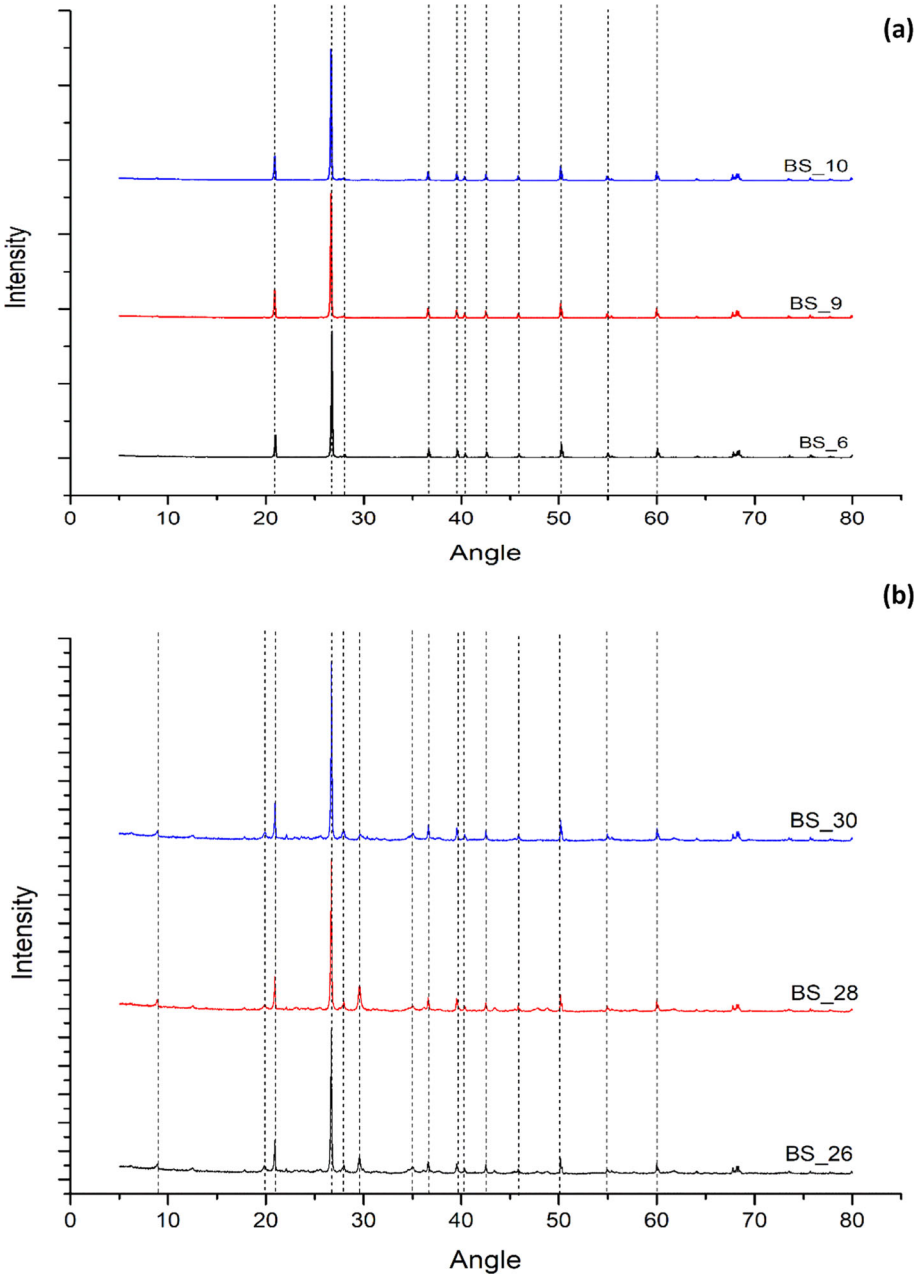

Figure 6. (**a** and **b**) XRD data for sand samples and the clay samples. Graphs clearly show the presence of quartz low and its peak is dominating another minerals peak.

particles. Yellow-coloured oxidised sand layers were also observed in unit 1. Unit 2 is around 0.4 m in thickness and has about 18–25% of silt, 75–80% of sand, and 1–2% of clay. Unit 3 is again 0.4 m thick fine sand with 95–98% of sand fraction, while 2–3% of silt is present. Unit 4 is 0.3 m thick and has a much more fraction of silt than unit 3, which is below it. Silt is about 18–25% in this unit. Unit 5 is 0.6 m thick, is dominated by finer sand particles, and is again a sandy layer. Unit 6 is 0.8 m thick and is composed of 18–20% of silt, 4–5% of clay, and 70–80% of sand. Unit 7 is 0.2 m thick and is a silt-dominated unit with 10–15% clay, 70–80% silt, and 10–20% of sand-sized particles. Unit 8 is 0.2 m thick and again has more silt (60–70%) percentage than sand (15–25%); however, the clay percentage is lesser than in unit 7. Unit 9 is 1.65 m thick and is dominated by clayey silt, which has 10–15% of clay. Reddish brown silty clay of this unit is rich in calcareous white nodules. Above unit 9 lies $\sim$0.35 m thick pottery-dominated horizon, mixed with black to light brown scree, which indicates human inhabitation and is considered as the cultural layer.

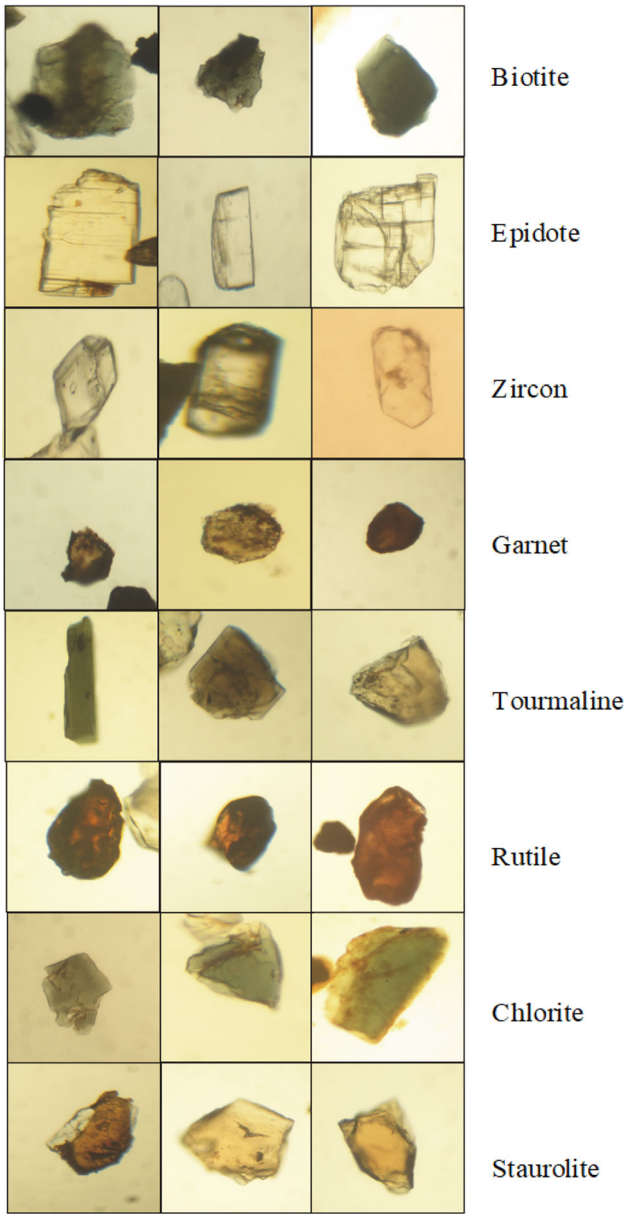

Figure 7. Heavy minerals present in the paleochannel. Pictures clearly show sub-angular to sub-rounded crystals.

4.2 *Texture analysis*

The variation in the mean size value of the data reveals that samples consist of very fine sand to medium silt sediments having 10–16% clay mixed with medium silt samples (figure 5). Silt samples present in unit 9 of the sequence are bimodal and trimodal, poorly sorted, and mesokurtic to very leptokurtic in nature. The sediments from units 8 and 7 of the sequence are unimodal and finely skewed. Fine sand samples of units 1 and 3 of the sequence show well-sorted grains which are near-symmetrical and mesokurtic in nature. Sorting in this unit is attributed to the recycling and transportation of the sediments. The interrelationship of various parameters shows the unimodal to bimodal nature of sediments (table 1).

4.3 *Chronology*

OSL dating has been done on four samples. The bottom-most sample from unit 1 has provided an age of 3.3 ± 0.2 ka. Second sample was taken from unit 6 of the section with silty sand lithology, which yielded the oldest date of the section, i.e., 11.2 ± 0.9 ka. The third sample was taken from the sand lithology of unit 7, which had given the age of 7.4 ± 2.4 ka. The top sample from unit 9 has given the age of 7.3 ± 0.7 ka (table 2).

4.4 *Mineralogy and geochemistry*

4.4.1 *Mineralogy*

X-ray diffraction (XRD) for 23 samples was used to scrutinise detailed mineralogy. These 23 samples represent the textural variations of the whole section. The bulk mineralogy of palaeochannel sediments mainly consists of quartz, K-feldspar, plagioclase, micas, and clay minerals (illite, chlorite, and montmorillonite) (figure 6). K-feldspar, with an abundance of quartz, is mostly present in the sand samples (figure 6a) and clay mineral illite is dominant in clayey-silt samples (figure 6b), showing the presence of water or humid climate after deposition (Keller 1962). The XRD pattern's variance in peak height may have been principally controlled by increasing quartz content (coarser fraction) in the samples; maybe it would have prohibited the other constituent minerals' peak heights from rising (figure 6a, b). Heavy minerals are significant provenance indicators and are also sensitive to weathering, transportation, deposition, and diagenesis (Morton 1985a, b). Heavy mineral assemblages of the palaeochannel mainly consist of tourmaline, zircon, garnet, staurolite, epidote, rutile, chlorite, and biotite. Garnet comprises the maximum percentage in the area followed by zircon, epidote, and tourmaline (figure 7). Zircon grains are of euhedral shape. The zircon-tourmaline-rutile index (ZTR index; Hubert 1962) was determined using the relationship ZTR Index = [(Z+T+R)/Non-opaque]. The ZTR index is 47%, indicating that the sediments were moderately weathered (figure 8).

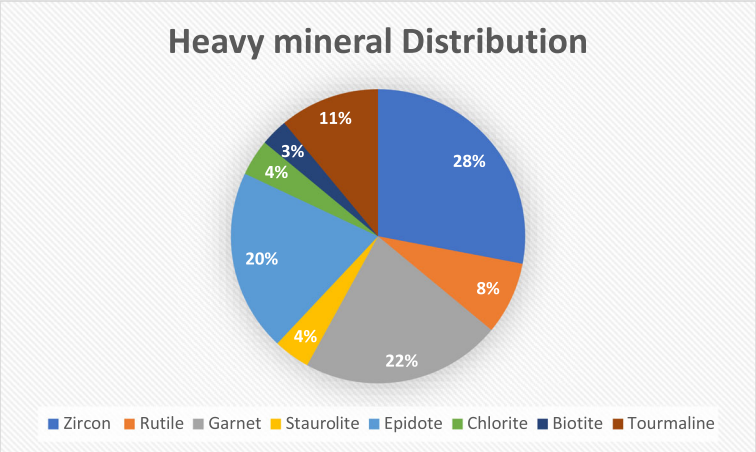

Figure 8. Diagram showing the percentage of heavy minerals in the paleochannel. The zircon–tourmaline–rutile index comes out to 47%.

4.4.2 *Geochemistry*

Identification of provenance, weathering of the source area, and tectonics can be done through the chemical composition of the clastic sediments (Pettijohn 1972; Bhatia 1983, Bhatia and Crook 1986; McLennan and Taylor 1983; Wornkiewicz and Condie 1987; Fedo *et al.* 1996; Nesbitt *et al.* 1996; McCann 1998; Singh and Rajamani 2001a, b; Tripathi and Rajamani 2003). The major elemental geochemistry of the sediments is given in table 3. The concentration of SiO_2 and Al_2O_3 in bulk sediments varies from ∼50 to 85 wt% and ∼10 to 18 wt%, respectively. Fe_2O_3 (∼2–8 wt%) and MgO (∼0.5–2.5 wt%) show good variance. MnO (∼0.02–0.11 wt%), TiO_2 (∼0.2–0.7 wt%), P_2O_5 (∼0.1–0.3 wt%), K_2O (∼1.8–3.5 wt%), and Na_2O (∼0.2–1 wt%) are in restricted ranges, CaO (∼0.4–10.8 wt%) show large variation (table 3, figure 9). Cross plots (figure 10) of major oxides with Al_2O_3 show that there is a positive correlation with other major oxides such as TiO_2 ($r = 0.89$), Fe_2O_3 ($r = 0.97$), K_2O ($r = 0.98$), and MgO ($r = 0.91$), where the increasing trend of these elements probably points towards enhancement of clay minerals (Nagarajan *et al.* 2007a, b). A negative association with SiO_2 ($r = 0.93$) and Na_2O ($r = 0.53$) indicates that the sediments come from well-developed continental provenance. Enrichment of Al and Fe points towards the formation of clay minerals, mainly of 2:1 type (illite) (Keller 1970a, b). Depletion of Na more than K shows the alteration of plagioclase feldspar. Compared to Na, Ca is not depleted much; however, this may result from secondary carbonate formation demonstrated by the stepwise loss on ignition (LOI) values (table 3). The concentration of TiO_2 is more in clayey silt (≤0.7) as compared to sands (≤0.03), suggesting less amount of phyllosilicate minerals in sands (Dabard 1990; Condie *et al.* 1992; Nagarajan *et al.* 2007a). Major REE and trace elements have a positive correlation with the grain size distribution. The amount of trace element values is given in table 4. Cr ($r = 0.4$), Co ($r = –0.9$), V ($r = 0.9$), and Cu ($r = 0.8$) have lesser values in the sediment samples compared to NASC and PAAS, but are associated with Al_2O_3 positively, indicating their association in clay-rich sediments (Wronkiewicz and Condie l987). Charts of the rare earth elements that have been chondrite-normalised (figure 11) show that the concentration of LREE (light rare earth elements) is much higher than HREE (heavy rare earth elements). The negative Eu anomalies are just like the values of UCC (McLennan *et al.* 2001). Values of HREE do not form a consistent or parallel pattern with the UCC, PAAS, or NASC (figure 11), which can result from the grain size effect (Taylor and McLennan 1985). Moreover, the concentration of HREE is less in sand-size samples, which may be credited to the quartz dilution effect (Götze and Lewis 1994).

5. Discussion

5.1 *Sediment maturity and source area weathering*

Sediment suites with various chemical compositions are often produced by the hydrological differentiating processes that take place on river sediments in combination with source rock composition and

Table 3. *Major oxide data for the sediment samples of the palaeochannel, along with the grain size data. Variation in LOI and CIA is also presented.*

Sample no.	Sand %	Silt %	Clay %	SiO_2	Al_2O_3	TiO_2	Fe_2O_3	MnO	MgO	CaO	Na_2O	K_2O	P_2O_5	LOI	CIA
bs-68	18.2	70.8	11.0	64.5	15.9	0.7	6.2	0.1	2.0	0.9	0.0	3.4	0.3	6.6	74.9
bs-66	5.7	79.5	14.8	59.9	16.7	0.7	6.7	0.1	2.0	0.9	0.0	3.5	0.3	7.4	75.5
bs-64	3.7	83.8	13.2	60.0	16.5	0.7	6.1	0.1	2.1	2.0	0.0	3.2	0.1	7.5	69.9
bs-62	4.0	80.8	15.2	59.5	16.9	0.7	6.2	0.1	2.2	3.1	0.0	3.3	0.1	8.7	64.7
bs-60	7.2	81.6	11.0	61.4	16.7	0.7	6.4	0.1	2.3	1.8	0.0	3.3	0.1	7.5	70.9
bs-58	6.8	80.8	12.4	58.2	17.2	0.7	6.6	0.1	2.4	3.2	0.0	3.3	0.1	9.2	64.7
bs-56	6.9	83.3	9.8	59.8	16.7	0.7	6.5	0.1	2.4	2.3	0.0	3.3	0.1	7.6	68.3
bs-54	6.6	84.8	9.0	50.7	15.6	0.6	4.9	0.1	2.4	10.8	0.0	3.1	0.1	13.4	40.4
bs-52	6.0	83.6	10.2	54.8	16.8	0.6	6.0	0.1	2.4	6.2	0.0	3.3	0.1	10.8	53.1
bs-50	17.2	65.0	7.9	61.3	16.7	0.7	6.2	0.1	2.3	2.4	0.0	3.3	0.1	7.3	67.8
bs-48	5.6	83.8	10.7	59.4	17.3	0.7	7.4	0.1	2.2	1.8	0.0	3.4	0.1	7.9	71.3
bs-46	83.6	14.2	2.1	63.2	13.9	0.6	5.0	0.1	1.4	0.6	0.1	2.7	0.1	12.4	76.9
bs-44	77.8	19.4	2.8	70.8	14.0	0.6	5.2	0.1	1.4	0.6	0.0	2.8	0.1	5.3	77.3
bs-42	81.0	16.0	2.7	72.2	12.9	0.6	4.7	0.1	1.3	0.6	0.2	2.6	0.1	4.8	75.3
bs-40	83.9	13.0	2.1	75.8	12.0	0.5	3.9	0.0	1.2	0.6	0.3	2.4	0.1	4.1	74.2
bs-38	91.5	7.3	1.2	80.3	10.3	0.4	2.5	0.0	1.0	0.5	0.7	2.1	0.1	2.2	70.4
bs-36	96.5	2.7	0.8	82.2	9.8	0.3	2.0	0.0	0.9	0.4	0.8	2.1	0.1	1.6	69.4
bs-34	97.0	2.6	0.6	81.0	10.1	0.3	2.4	0.1	1.0	0.5	0.7	2.2	0.1	1.8	69.5
bs-32	94.4	4.7	0.9	81.4	10.1	0.3	2.4	0.0	1.0	0.4	0.7	2.1	0.1	1.7	70.9
bs-30	75.3	21.9	2.7	80.9	10.0	0.4	2.5	0.0	1.0	0.5	0.7	2.1	0.1	1.9	69.8
bs-28	97.0	2.3	0.6	81.0	10.0	0.3	2.5	0.0	1.1	0.4	0.7	2.2	0.1	1.7	70.1
bs-26	92.1	3.0	1.1	78.9	10.9	0.5	3.2	0.0	1.1	0.5	0.6	2.2	0.1	2.8	71.8
bs-24	88.1	10.5	1.4	78.0	11.4	0.5	3.3	0.0	1.2	0.5	0.5	2.3	0.1	3.0	73.0
bs-22	90.2	8.4	1.3	79.2	10.6	0.4	2.9	0.0	1.0	0.5	0.6	2.2	0.1	2.5	71.2
bs-20	96.2	2.9	1.0	83.5	9.6	0.3	1.8	0.0	0.8	0.4	0.8	1.9	0.1	1.4	70.1
bs-18	97.7	1.6	0.7	82.5	9.4	0.3	1.8	0.1	0.7	0.4	0.9	1.9	0.1	2.1	68.8
bs-16	98.4	0.9	0.6	83.7	9.4	0.2	1.5	0.1	0.7	0.4	1.0	1.9	0.0	1.2	68.0
bs-14	95.9	3.3	0.9	82.1	9.9	0.4	2.2	0.0	0.9	0.5	0.7	2.0	0.1	1.7	70.1
bs-12	98.5	0.8	0.6	84.8	9.2	0.2	1.4	0.0	0.6	0.4	0.9	1.8	0.1	1.2	68.9
bs-10	98.5	0.8	0.6	83.8	9.3	0.2	1.5	0.0	0.8	0.4	0.9	1.9	0.1	1.3	68.6
bs-8	97.7	1.3	0.7	82.1	9.8	0.3	1.9	0.0	1.1	0.5	0.7	2.1	0.1	1.4	69.3
bs-6	98.4	1.1	0.6	84.7	9.3	0.2	1.4	0.0	0.8	0.4	0.9	1.9	0.1	1.0	68.6
bs-4	98.5	0.8	0.6	84.2	9.4	0.3	1.5	0.0	0.9	0.4	0.8	1.9	0.1	1.1	69.6
bs-3	99.8	0.2	0.0	84.6	9.5	0.2	1.3	0.0	0.9	0.4	0.9	2.0	0.1	1.0	68.5
bs-2	97.7	1.5	0.7	83.2	9.8	0.2	1.7	0.0	0.9	0.4	0.8	2.0	0.1	1.1	70.0
bs-1	96.8	2.5	0.8	83.1	9.8	0.2	1.6	0.0	0.9	0.4	0.9	2.0	0.1	1.1	69.1

chemical weathering (Nesbitt and Young 1989; Frallick and Kronberg 1997). As sediments become more mature, quartz replaces feldspar, mafic minerals, and lithic fragments in the sediments. As a result, the major elements Na, K, Ca, Al, Fe, Mg, and certain other trace elements are reduced, and SiO_2 is increased in the bed load sediments. Some ratios, such as SiO_2/Al_2O_3, Na_2O/K_2O, Fe_2O_3/K_2O, and Fe_2O_3/SiO_2, which serve as effective markers of sediment maturity, are impacted by this (Pettijohn *et al.* 1972; Herron 1988). SiO_2/Al_2O_3 ratios rise together with sediment maturity, whereas Fe_2O_3/SiO_2 and Al_2O_3/SiO_2 ratios fall. The ratios Na_2O/K_2O and Fe_2O_3/K_2O help in predicting the stability of feldspar and minerals bearing Fe and K. The sediments of the study area are plotted between $\log(Na_2O/K_2O)$ *vs.* $\log(SiO_2/Al_2O_3)$ (Pettijohn *et al.* 1972), which show that several of the sediments are arkosic (figure 12). Units 9 and 7 of the section is clay enriched and falls in the arkosic field, and the extremely low Na_2O/K_2O ratio due to *in situ* chemical weathering of clay enriched units 9 and 7 may be the reason for shifting the samples towards the arkosic field. Sand sediments fall in the

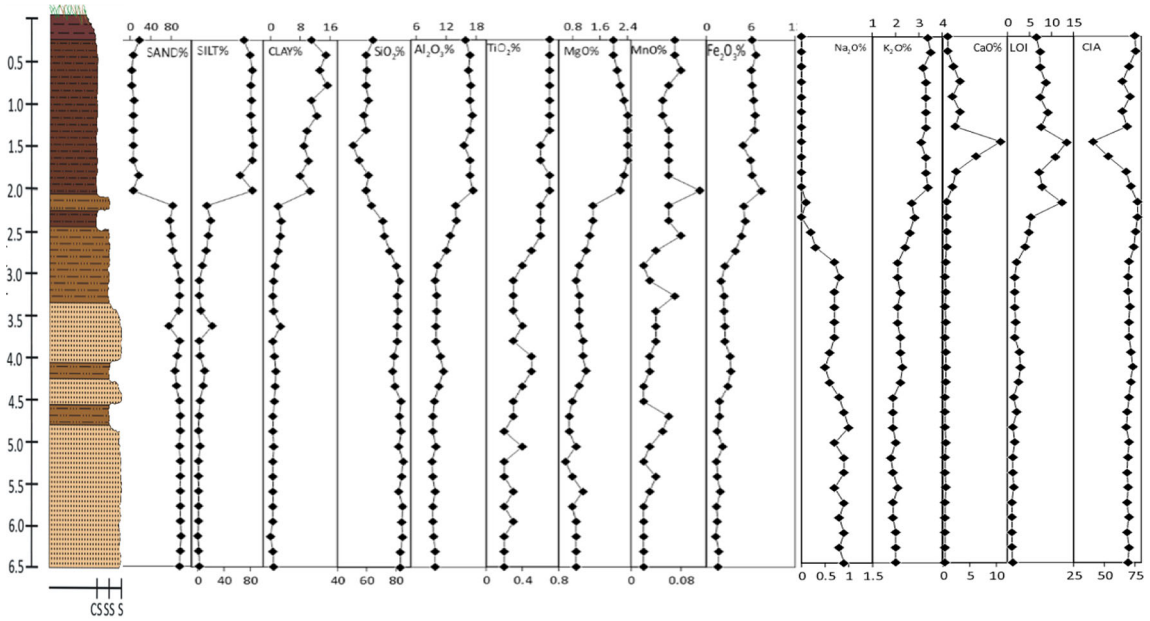

Figure 9. Grain size (sand, silt ± clay) distributions in the palaeochannel profile along with the litholog. Note that SiO_2 and felsic components are more in the coarser mode (sand), whereas mafic components are enriched in the finer sediments.

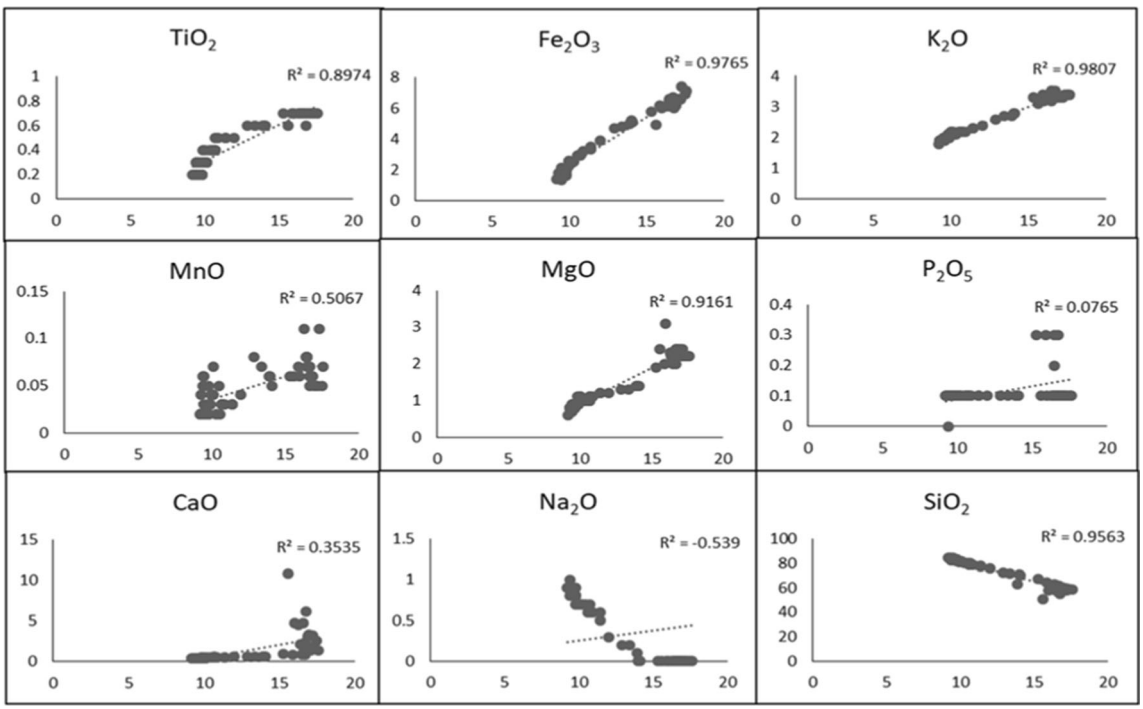

Figure 10. Cross plots of major oxides with Al_2O_3 show that there is a positive correlation of major oxides like TiO_2 ($r = 0.89$), Fe_2O_3 ($r = 0.97$), K_2O ($r = 0.98$), MgO ($r = 0.91$), whereas SiO_2 ($r = –0.93$) and Na_2O ($r = –0.53$) show negative correlation.

litharenite segment inferring more physical weathering or less alteration of feldspar (Singh 2010). Graph Fe_2O_3/K_2O (Heron 1988) shows that arkosic arenites are grading into shale with wackes in transition (figure 12) units of the section with high silt and clay percentage are having high Fe_2O_3/K_2O ratio and the negative relation of SiO_2 with Fe, Mn, and Ti point towards the weathering of the sediments. This can be attributed to the mature and recycled nature of the sand grains (Bhatia 1983) as well as the formation of illite clay minerals.

The value of Pb corresponds to the grain size effect (Vital *et al.* 1999a, b) and, therefore, is found higher in the clay-rich sediments than the value of PAAS and the value is less in the sand-rich

Table 4. *Trace and rare earth element (REE) data (ppm) for the palaeochannel sediments.*

Sample no.	V	Cr	Co	Cu	U	Sc	Y	Th	∑LREE	∑HREE	La	La/ Th	∑LREE/ ∑HREE	Th/ U
bs-68	117.1	75.3	50.3	37.3	3.3	13.3	17.2	14.2	77.6	6.3	41.5	2.9	10.8	4.3
bs-66	120.1	144.2	35.0	39.0	3.5	14.7	21.0	15.9	80.1	6.9	41.6	2.6	12.5	4.5
bs-64	113.5	126.3	33.0	31.1	3.6	12.7	19.2	15.3	66.8	5.5	42.9	2.8	10.5	4.3
bs-62	122.5	70.2	34.3	32.0	3.7	14.3	20.9	17.9	77.2	6.5	48.2	2.7	10.0	4.8
bs-60	125.7	134.7	38.4	34.8	4.6	15.0	22.5	17.9	208.9	17.9	47.9	2.7	11.3	3.9
bs-58	127.6	145.6	31.4	35.4	5.3	14.5	24.7	17.0	188.8	16.5	48.4	2.9	11.6	3.2
bs-56	102.0	162.8	33.9	35.2	5.0	14.0	22.1	16.3	179.4	16.5	46.4	2.8	11.2	3.3
bs-54	105.6	135.3	40.7	31.0	5.2	12.8	24.4	15.3	180.1	15.1	45.4	3.0	10.6	2.9
bs-52	113.1	139.7	31.2	34.0	5.6	13.1	21.2	15.8	207.6	19.1	45.8	2.9	10.8	2.8
bs-50	86.6	110.3	40.9	40.0	4.0	13.6	20.3	21.9	212.5	17.0	48.9	2.2	11.8	5.4
bs-48	90.1	50.3	61.1	25.6	3.2	8.8	14.8	12.5	200.6	19.1	40.9	3.3	10.8	3.9
bs-46	86.0	54.5	71.7	23.2	3.2	10.3	18.1	15.2	195.4	19.6	41.3	2.7	11.3	4.7
bs-44	63.1	53.8	107.8	19.0	2.8	8.4	19.7	14.4	200.9	18.8	35.4	2.5	11.7	5.1
bs-42	45.8	84.2	155.6	13.0	2.2	4.9	13.3	9.7	208.3	19.7	29.0	3.0	11.0	4.3
bs-40	33.1	24.1	214.6	7.0	1.4	4.0	10.2	7.7	209.7	18.6	20.1	2.6	9.9	5.5
bs-38	31.2	46.3	202.4	6.9	1.4	3.1	8.8	6.3	201.3	17.4	19.1	3.0	11.3	4.6
bs-36	36.5	26.1	205.6	6.3	1.3	3.7	8.4	5.6	208.9	18.7	17.6	3.2	11.6	4.2
bs-34	42.0	24.4	190.4	8.0	1.5	4.0	7.8	6.0	109.9	10.4	19.6	3.3	11.2	4.0
bs-32	42.1	75.0	174.6	9.3	1.6	3.9	9.4	6.5	94.9	8.8	21.6	3.3	12.1	4.1
bs-30	41.7	64.3	195.7	10.0	1.7	4.5	12.8	8.8	86.2	7.3	25.0	2.8	12.4	5.2
bs-28	141.1	144.9	38.6	37.8	5.2	16.1	22.5	17.3	77.1	7.2	47.7	2.8	11.8	3.4
bs-26	40.0	19.3	150.0	48.1	1.6	4.4	9.9	7.0	81.9	7.3	20.4	2.9	12.3	4.3
bs-24	53.6	31.7	144.9	13.1	2.6	6.4	15.6	12.6	87.8	7.5	31.8	2.5	11.6	4.8
bs-22	49.0	28.0	122.5	11.3	2.0	5.5	13.5	10.2	124.6	11.3	29.2	2.9	12.2	5.1
bs-20	49.1	32.6	127.5	11.4	2.5	5.4	14.1	11.0	154.6	15.6	32.3	2.9	11.8	4.4
bs-18	32.3	19.6	167.4	6.8	1.4	3.5	9.8	8.3	179.9	16.0	23.7	2.8	11.1	6.0
bs-16	26.8	12.7	203.0	4.6	1.0	2.7	7.3	5.5	176.0	15.2	16.8	3.0	10.8	5.4
bs-14	31.0	18.4	184.6	5.2	1.5	3.0	9.2	6.6	95.8	8.6	23.9	3.6	11.7	4.5
bs-12	35.3	428.3	214.7	16.3	1.6	3.9	11.3	9.3	110.1	9.1	25.1	2.7	11.4	5.7
bs-10	27.7	15.2	231.2	4.1	1.3	3.6	12.5	8.7	104.6	8.5	22.1	2.5	10.8	6.6
bs-8	44.2	63.1	192.2	8.3	1.6	3.3	7.5	5.4	72.0	6.9	17.5	3.3	10.5	3.4
bs-6	34.5	23.4	154.4	6.9	1.3	2.3	6.1	4.4	103.7	8.8	18.1	4.1	11.8	3.5
bs-4	25.8	81.0	178.6	7.2	1.0	3.1	9.3	6.8	139.2	12.0	15.6	2.3	11.6	6.6
bs-3	27.1	21.6	181.9	5.1	1.3	2.8	7.2	5.8	126.1	12.9	18.7	3.2	9.8	4.5
bs-2	27.4	22.6	123.9	4.9	1.1	3.1	8.6	6.1	138.7	12.7	18.3	3.0	10.9	5.8
bs-1	25.5	17.5	111.0	4.7	1.0	2.5	7.0	4.5	89.5	8.5	17.2	3.8	10.6	4.5

sediments. A similar pattern is observed with V, Cr, U, Sc, Y, and Th, clearly showing the quartz dilution effect (Götze and Lewis 1994) in the sand-rich samples, affecting the absolute values of all other elements. LREE are positively correlated to the Al_2O_3, specifying that these are dominantly related to the clay minerals (Taylor and McLennan 1985). UCC and PAAS normalised plots of sediments show variation in the Eu anomaly values. Coarser grain size sediments have positive Eu anomalies, while clay size sediments show negative Eu anomalies; it might happen if the source location experiences less chemical weathering (Middelburg *et al.* 1988) as well as retention of feldspar in the sediments responsible for positive Eu anomaly. Moreover, the sand samples have not undergone much mineralogical sorting could also be the reason for the positive Eu anomaly (Bhatia 1985; Singh and Rajamani 2001a, b).

During weathering, smaller cations like Sr, Ca, and Na, deplete in the initial stage; however, the larger cations (Al and Rb) remain immobile, rather enriched in due course of time (Nesbitt and Young 1982, 1984; McLennan *et al.* 1993; Fedo *et al.*

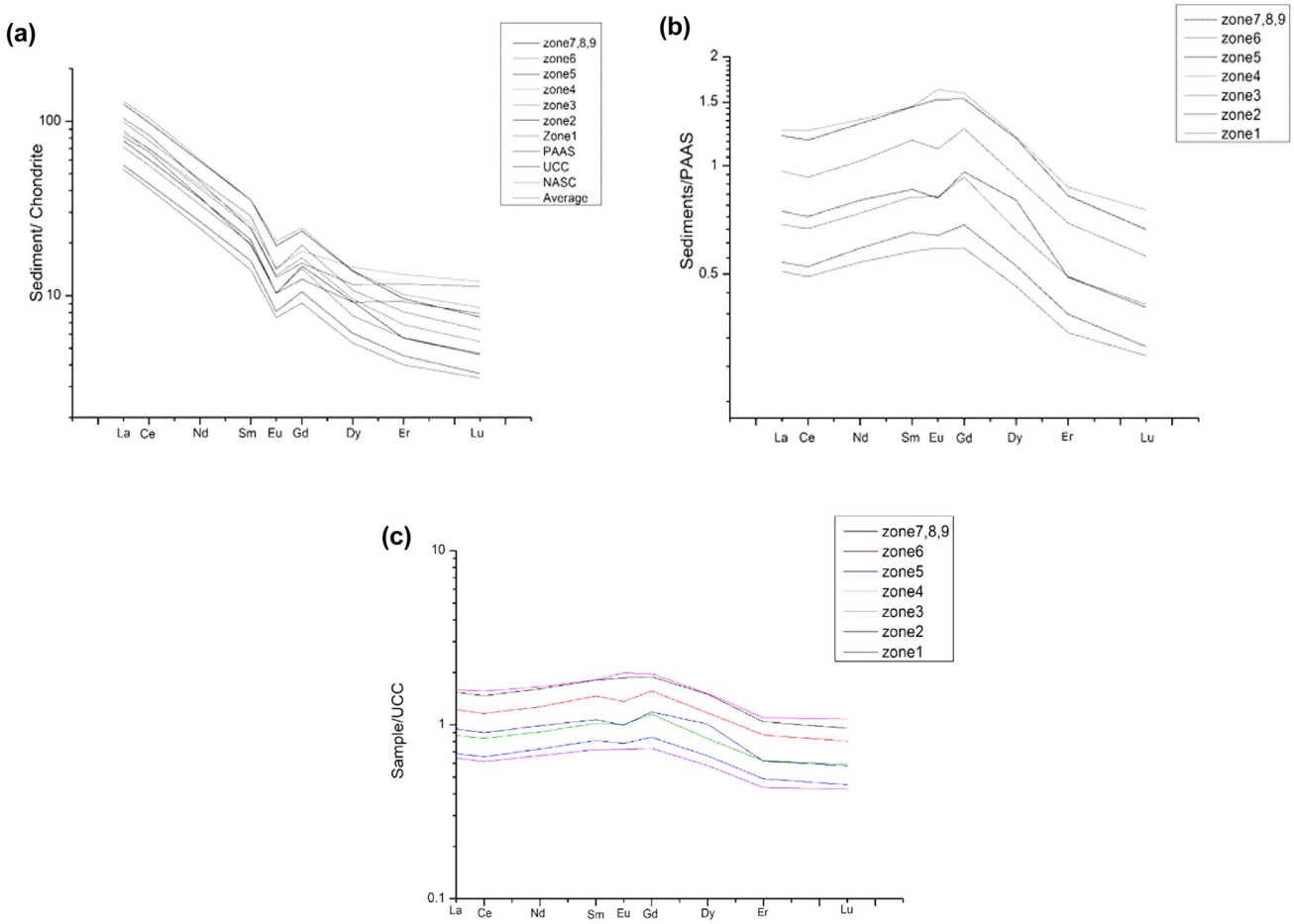

Figure 11. **(a)** Chondrite normalised samples are plotted to compare with UCC, PAAS and NASC. The pattern shows negative Eu anomaly. (**b** and **c**) PAAS and UCC normalised samples showing a similar pattern with positive Eu anomaly for one or two samples. Sources: chondrite (McDonough and Sun 1995), UCC (Rudnick and Gao 2003) and PAAS (Taylor and McLennan 1985).

1995). To determine the degree of weathering, CIA is commonly used (Nesbitt and Young 1982), where CIA = $\{Al_2O_3/(Al_2O_3 + CaO^* + Na_2O + K_2O)\} \times 100$ (*CaO in silicate fraction only). In the current study, CIA values range from 63 to 77. Al_2O_3, Na_2O, and CaO* are displayed in the A–CN–K ternary diagram to assess the migration of the elements throughout the development of chemical weathering. It has been observed that the sediment samples plot over the plagioclase–K-feldspar line. The A–CN–K plot shows that most of the fall at the A–K edge as they approach the illite composition denotes moderate weathering (figure 13). When analysing the constitution of the source rock, the A–CN–K ternary plot excels because it may be projected backward and parallel to the A–CN line of weathered samples up to a position on the feldspar connect (Fedo *et al.* 1995; Tang *et al.* 2012). Siliciclastic sediments of the current research are found to be derived from granite as a probable source and to extend up to the illite stability zone beside a trend line parallel to the A–CN axis. Thus, the diagram implies that samples originated from granitic rocks as the source is influenced by weak chemical weathering (Madhavaraju *et al.* 2016). Moreover, figure 13 also shows that the major Himalayan rivers' sediments plot in the zone of weak weathering (CIA = 55–65), whereas the Ghaggar sediments show an intermediate degree of weathering (CIA = 69). Overall, the intermediate CIA values (63–77) for the palaeochannel sediments indicate semi-arid, water-starved granitic sources. Further, the textural attributes support physical weathering with a tectonic control.

5.2 *Provenance of sediments*

In the current study, the LREE values are much higher than HREE and do not form a consistent or parallel pattern with the PAAS or NASC (Taylor

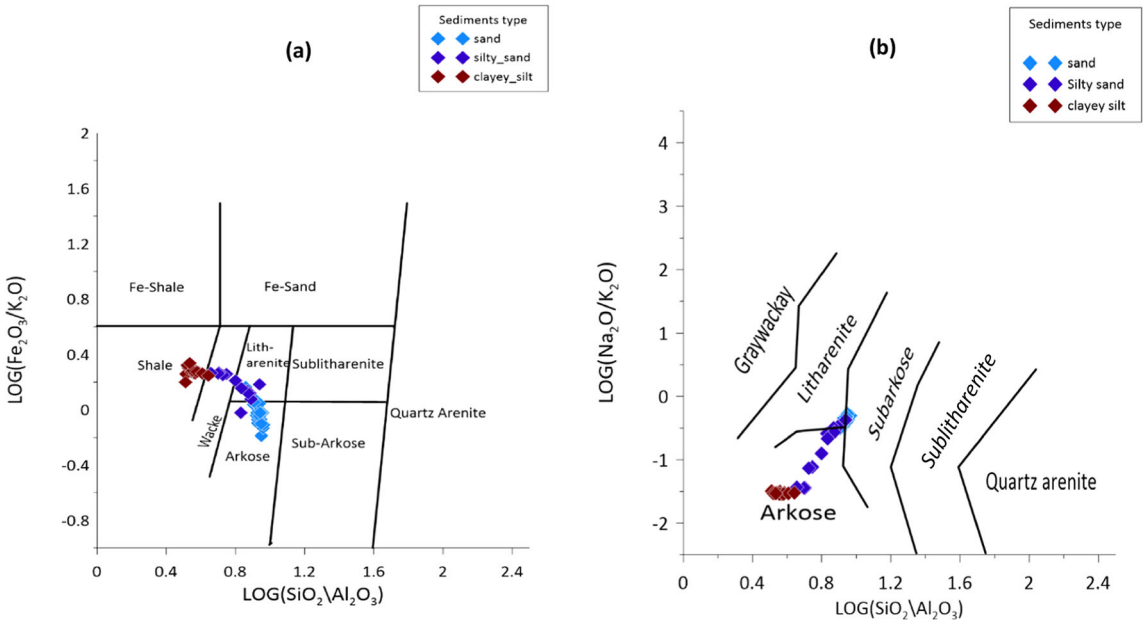

Figure 12. Plot of sediments on the geochemical classification diagrams after Herron (1988) **(a)** $\log(Fe_2O_3/K_2O)$ *vs.* $\log(SiO_2/Al_2O_3)$ and **(b)** $\log(Na_2O/K_2O)$ *vs.* $\log(SiO_2/Al_2O_3)$ (Pettijohn *et al.* 1972). Diagrams are clearly showing that the sediments which are dominated by sand lies in arkose field, silt dominated part lies in wacke field and clay dominated part lies in shale field.

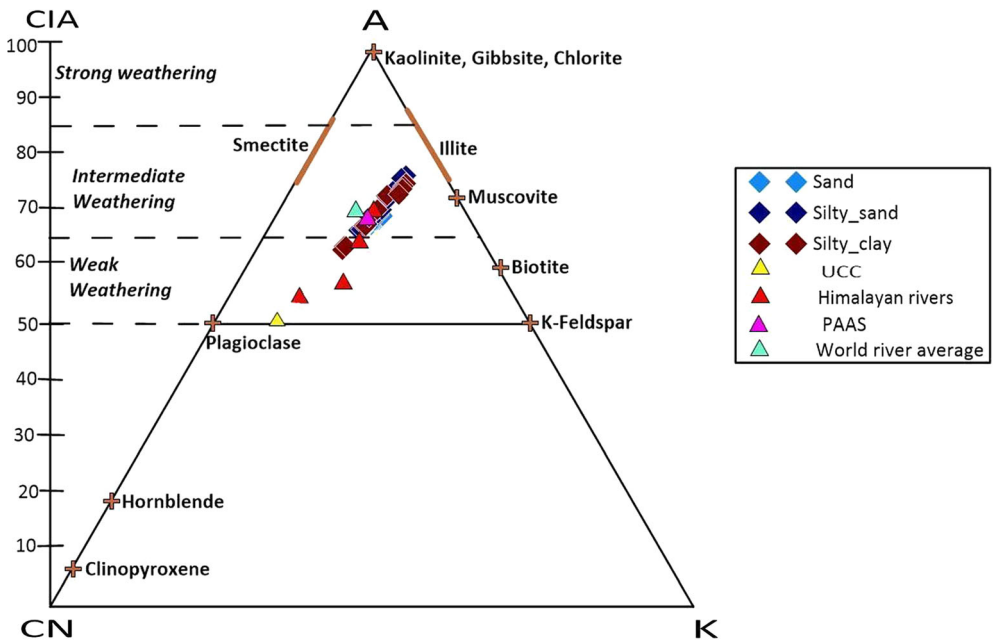

Figure 13. A–CN–K ternary plot (Nesbitt and Young 1982) showing chemical maturity of paleochannel sediments. Also shown for comparison are modern river sediments from Himalaya, average values for world river sediments (Li and Yang 2010), UCC, and PAAS.

and McLennan 1981), which may result from the grain size effect (Taylor and McLennan 1985). In our samples, LREE are more positively correlated to Al_2O_3, indicating that these are dominantly connected to the clay minerals. It is intriguing to observe that coarser sediments normalised with PAAS and NASC show positive Eu anomaly with lower HREE abundance, probably indicating the dominance of physical weathering over chemical weathering in the source region. As opposed to

Table 5. *Correlation coefficients (r) from correlation matrix obtained with mineralogical and geochemical data of palaeochannel sediments.*

∑LREE/ ∑HREE	La/Th	La	∑HREE	∑LREE	Th	Y	Sc	U	Cu	Co	Cr	V	K_2O	Na_2O	CaO	MgO	MnO	Fe_2O_3	TiO_2	P_2O_5	Al_2O_3	SiO_2	
0.1	−0.1	−0.9	−0.1	−0.1	−0.8	−0.8	−0.9	−0.9	−0.9	0.9	−0.4	−0.9	−1.0	1.0	−0.7	−1.0	−0.7	−1.0	−0.9	−0.3	−1.0	1.0	SiO_2
−0.1	0.1	1.0	0.0	0.1	0.8	0.8	0.9	0.9	0.9	−0.9	0.4	1.0	1.0	−1.0	0.5	1.0	0.7	1.0	1.0	0.3	1.0		Al_2O_3
0.2	−0.1	0.3	−0.4	−0.3	0.3	0.3	0.4	0.3	0.4	−0.3	0.2	0.4	0.4	−0.4	0.0	0.3	0.3	0.4	0.4	1.0			P_2O_5
0.0	0.1	1.0	0.0	0.0	0.9	0.9	0.9	0.9	0.9	−0.9	0.4	1.0	1.0	−1.0	0.5	0.9	0.7	1.0	1.0				TiO_2
0.0	0.1	1.0	0.0	0.0	0.8	0.8	0.9	0.9	0.9	−0.9	0.4	1.0	1.0	−1.0	0.5	1.0	0.7	1.0					Fe_2O_3
0.1	0.1	0.7	−0.1	0.0	0.6	0.5	0.6	0.6	0.7	−0.6	0.5	0.6	0.7	−0.7	0.4	0.7	1.0						MnO
−0.1	0.1	0.9	0.0	0.0	0.8	0.8	0.9	0.9	0.9	−0.9	0.5	1.0	1.0	−0.9	0.6	1.0							MgO
−0.2	0.0	0.5	0.1	0.2	0.5	0.6	0.5	0.6	0.5	−0.5	0.3	0.5	0.5	−0.5	1.0								CaO
0.0	−0.1	−1.0	−0.1	−0.1	−0.8	−0.8	−0.9	−0.9	−0.9	0.9	−0.4	−1.0	−1.0	1.0									Na_2O
0.0	0.1	0.9	0.0	0.0	0.8	0.8	0.9	0.9	0.9	−0.9	0.4	1.0	1.0										K_2O
0.0	0.1	0.9	0.0	0.0	0.8	0.8	0.9	0.9	0.9	−0.9	0.4	1.0											V
0.1	0.1	0.4	−0.1	−0.1	0.4	0.4	0.4	0.5	0.4	−0.3	1.0												Cr
0.0	−0.1	−0.9	−0.1	−0.1	−0.8	−0.8	−0.9	−0.9	−0.8	1.0													Co
0.1	0.1	0.8	−0.1	0.0	0.8	0.7	0.8	0.8	1.0														Cu
0.0	0.1	0.9	0.1	0.1	0.8	0.9	0.9	1.0															U
0.0	−0.3	0.9	0.1	0.1	0.9	0.9	1.0																Sc
0.1	−0.3	0.9	0.2	0.2	1.0	1.0																	Y
0.1	−0.4	0.9	0.2	0.2	1.0																		Th
−0.2	−0.2	0.1	1.0	1.0																			∑LREE
−0.2	−0.2	0.1	1.0																				∑HREE
0.0	0.1	1.0																					La
−0.1	1.0																						La/Th
1.0																							∑LREE/ ∑HREE

that, the samples of the sandy silt and clayey silt texture show negative Eu anomaly, which could result from plagioclase weathering at the deposition site. There is a positive association between LREE and Th, indicating felsic lithologies may have contributed (McLennan *et al.* 1980). The La/Th value ranges between 2.30 and 4.01, usually similar to UCC and PAAS, respectively, clearly indicating the grain size bias where coarser sediments are associated with granitoid and relatively finer sediments are of intermediate composition. A positive correlation is shown by REEs (table 5) to some extent with the other major oxides like MgO_2, TiO_2, and Fe_2O_3, however, they show a negative correlation with trace elements like Cu, Co, Cr, and U, showing the contribution of REEs from mica biotite and chlorite minerals (Taylor and McLennan 1985; Bauluz *et al.* 2000). La–Th–Sc ternary plot (Singh 2010) has been drawn to infer the provenance (figure 14). All the sediments fall in between the composition of granite and granodiorite.

We have also applied the discriminant function scheme (figure 15) of provenance estimation proposed by Roscher and Korsch (1988). In the current study, sediments fall in the P4 part with a little shift towards the P1 part; this could be the result of the grain size effect (Whitmore *et al.* 2004). The shifting of results seen in this study is relatable to the study carried out by Roscher and Korch (1988) on sedimentary rocks of the Ordovician and the Silurian greywacke having $SiO_2 >$ 70%, where coarser sediments fall in P4 and finer sediments fall in P1 and P2 fields. The greywackes used in Roscher and Korch's (1988) study may be produced by the successive recycling of older sediments (Wyborn and Chappel 1983) and the composition of quartzose sedimentary sources can most probably be derived from varied sedimentary litho units and detrital components of different crystalline rocks. Similar results have been obtained in our study, as the sediments we have taken are also reworked having $SiO_2 > 70\%$ and probably produced by successive recycling of older sediments.

Heavy-mineral assemblages of terrigenous sediments also help in establishing the source of sediments (Carroll 1953; Crook 1968; Cleary and Conolly 1972; Colin *et al.* 1993; Oliva *et al.* 1999; Thomas *et al.* 1999; Horbe *et al.* 2004; Van Loon and Mange 2007). In the present study, the ZTR index is 46%, indicating that the sediments are moderately weathered and additionally corroborated by the CIA readings. The presence of garnet

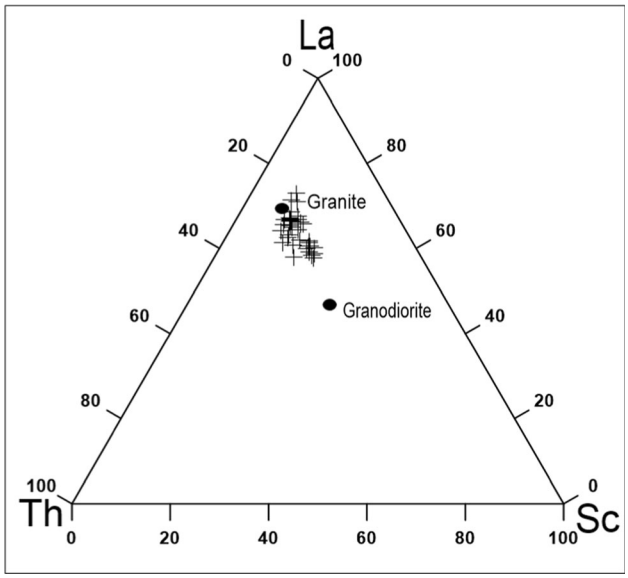

Figure 14. La–Th–Sc ternary plot after Singh (2010) showing the composition of the source rock lies in between the granite and granodiorite.

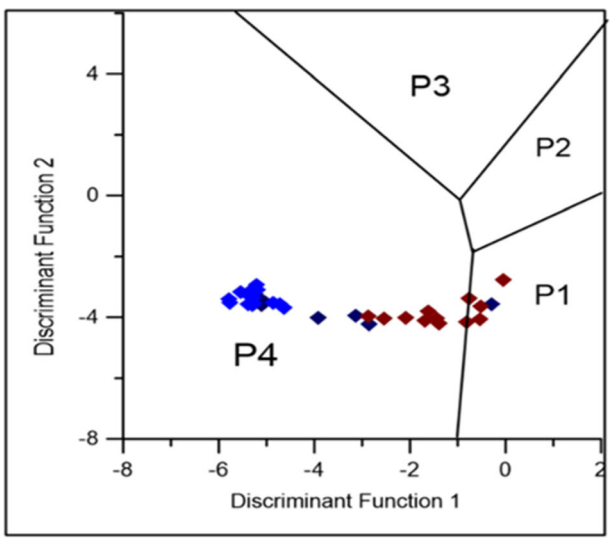

Figure 15. Discriminant function 1 against discriminant function 2 variation diagram. Fields after Roser and Korsch (1988), wherein F1 = $-1.733TiO_2 + 0.607Al_2O_3 + 0.76Fe_2O_3 - 1.5MgO + 0.616CaO + 0.509Na_2O - 1.224K_2O - 9.09$, and F2 = $0.445TiO_2 + 0.07Al_2O_3 - 0.25Fe_2O$. Provenance fields: (P1) mafic igneous provenance, (P2) intermediate igneous provenance, (P3) felsic igneous provenance, and (P4) quartzose sedimentary provenance.

and epidote also shows the unweathered nature of the sediments (Hester 1974). Zircon grains present are of a euhedral shape and are derived from acidic igneous rocks (Basu 1985). All the grains are mostly sub-rounded to rounded showing their involvement in cyclic transportation (Pettijohn *et al.* 1973). The mixing of results led us to plot sediment bivariant plots (figure 16a, b, c, and d)

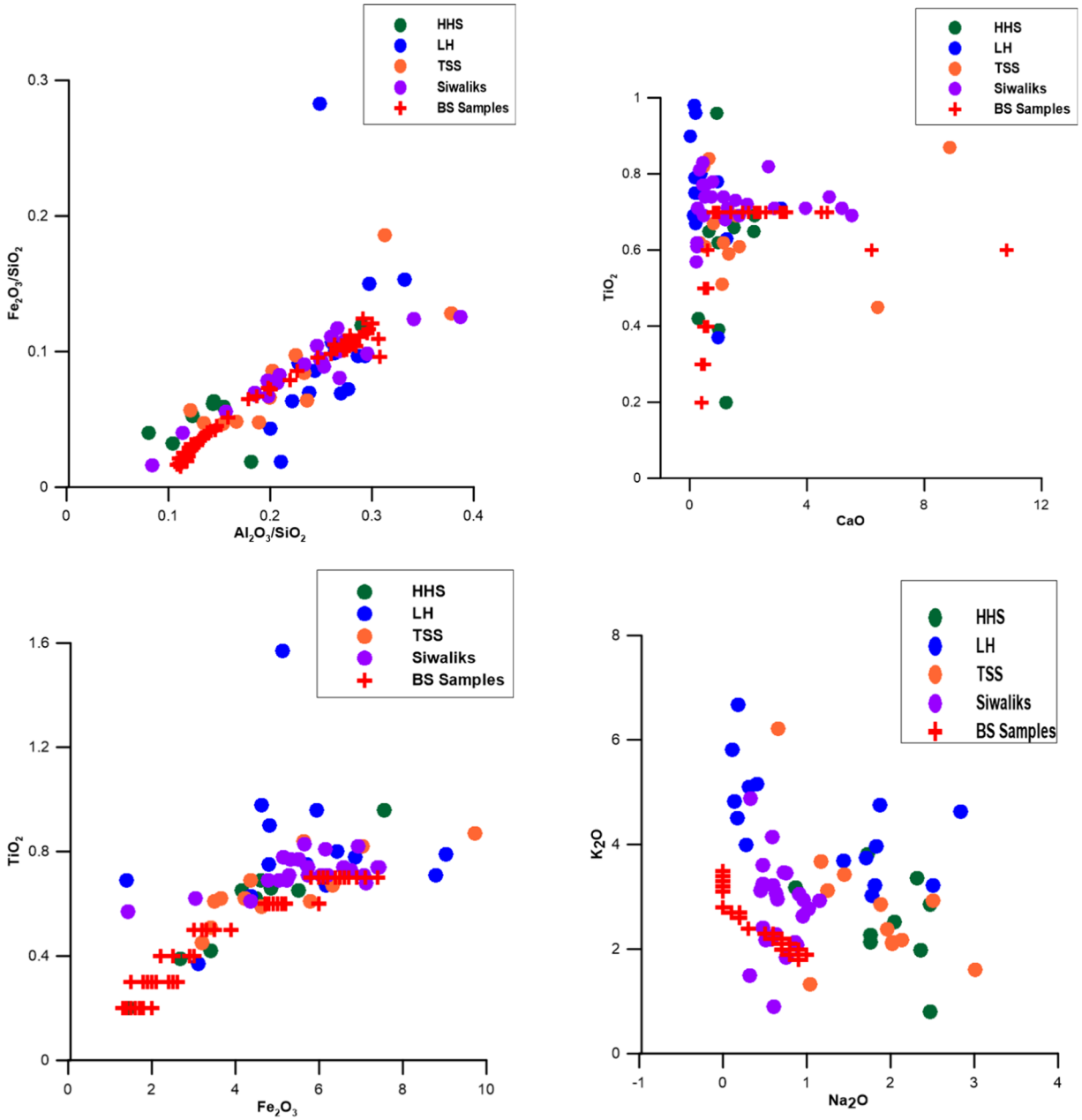

Figure 16. Sediment bivarent plots after Singh (2010). Values of Tethyan Sedimentary Series (TSS), High Himalayan Series (HHS) and Lesser Himlayan Series have been taken from Richards *et al.* (2005) and Siwaliks has been taken from Sinha *et al.* (2007). The above plots indicate the sediments are mostly deviated towards Siwaliks.

(Singh 2010). Values of the Tethyan Sedimentary Series (TSS), High Himalayan Series (HHS), and Lesser Himalayan Series have been taken from Richards *et al.* (2005) and Siwaliks have been taken from Sinha *et al.* (2007). The above plots indicate the sediments mostly deviated towards Siwaliks. Siwaliks are formed from LHS and HHS (Sinha *et al.* 2007); therefore in the current study, the samples are also showing mixed geochemistry of the Himalayan ranges.

5.3 *Tectonic setting*

Any sedimentary basin's tectonic context can be distinguished based on geochemistry (Bhatia 1983, 1984, 1985a; Roser and Krosch 1986; McLennan and Taylor 1991; Graver and Scott 1995). To ascertain the tectonic setting, discrimination diagrams (figure 17) suggested by Roser and Korsch (1986) and K_2O/Na_2O–SiO_2/Al_2O_3 relationship diagrams (after Maynard *et al.* 1982) were

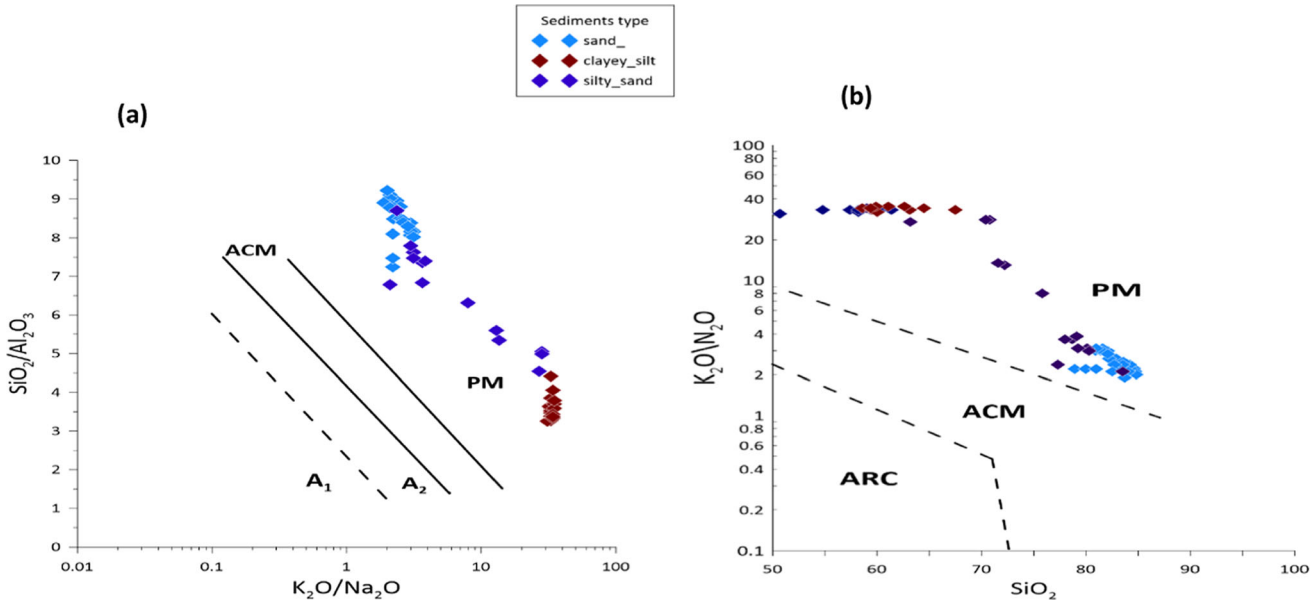

Figure 17. Tectonic discrimination diagram **(a)** Roser and Korsch (1986) and **(b)** Maynard *et al.* (1982) samples plot in passive margin field (PM). ACM = active continental margin field, ARC = continental arc sediments plot in (PM) field. A1 = arc basaltic and andesitic detritus; A2 = evolved arc setting felsitic plutonic detritus.

applied. These illustrations imply that the samples were laid in a passive margin environment typified by mineralogically mature (quartz-rich) sediments probably brought by rivers to the deposition site. The northern Indian passive margin consists of the Higher and Lower Himalayas and a small part of the Indian craton and their sedimentary cover (Baud *et al.* 1996). The examined samples are located in the P4 field in the diagram showing a reworked orogenic landscape (quartzose sedimentary or granite-gneisses origin source region like PM) that was settled under the passive margin regime. The heavy mineral assemblages (discussed earlier also) clearly show that the sediments come from all parts of the Himalayas, including the Siwaliks, the lower Himalayas, and the upper Himalayas.

5.4 *Depositional environment and climatic changes*

Depositional environment of the sediments is well correlated with the climate change of the area. Unit 1 has current beddings and ripple marks, indicating a palaeochannel of a flowing river. The lower part of the section, i.e., units 1, 2, 3, and 5 containing sand-size grain particles are arkosic and are subjected to less chemical weathering as compared to the upper part of the section, i.e., units 6, 7, 8, and 9, comprising silt and clay, showing a much more matured part of the section. Units 7 and 8 have poorly sorted nature of the sediments with a high kurtosis value denoting that the depositional environment has less energy. Poorly sorted nature of sediments can be attributed to the *in-situ* chemical weathering condition of the depositional area. Overall textural characteristics show fining upward sequence and also point towards decreasing depositional energy conditions. Negative Eu anomaly similar to PAAS and UCC of the average sediments indicates some cratonic source of sediments. The positive correlation of REEs and major oxides like Al_2O_3, TiO_2, K_2O, MgO, and Fe_2O_3 shows that REEs are indicating towards the granitic source rock. The value of CIA is intermediate (63–77), inferring intermediate weathering of the sediments at the source area because of a higher rate of physical weathering over chemical weathering. The above data and OSL results reveal that the lower part comprising unit 1 is the youngest dating back to 3.3 ± 0.2 ka, which can result from an incision by some sudden flow of water resulting from some instant weather change. The upper part comprising unit 6 is the oldest (11.2 ± 0.9 ka) and units 7 (7.4 ± 2.4 ka) and 9 (7.3 ± 0.2 ka) are relatively mature in nature.

The texture, mineralogy, and geochemistry of sediments invoke that they are mature (mineralogical constraints), recycled (sub-rounded to rounded grains), and physically weathered

(arkosic). The sediment terrain is felsic in nature, having high-grade metamorphic rocks (heavy mineral assemblages), most probably granite or granitoid. Besides, the sediments are derived from a high altitude and arid climatic area. The climate change can be attributed to the chemically matured unit 6 dating back to 11.2 ± 0.9 ka with CIA values ranging from ∼69 to 70.5, with less percentage of Al_2O_3 and more of SiO_2 percentage, which can be due to low depositional energy with dry climatic conditions, whereas units 7 (7.4 ± 2.4 ka) and 9 (7.3 ± 0.2 ka) have CIA values of ∼75–77, more percentage of Al_2O_3 and less of SiO_2 percentage showing warm and humid climate. These phases correspond well with the records of lake proxies of the Ganga plain, where 14–12.5 ka and 11.5–10.5 ka are marked by cool and dry climate (Sharma *et al.* 2004; Chauhan *et al.* 2015) and period of 8.5–6.4 ka (Trivedi *et al.* 2013; Saxena *et al.* 2015) has a warm and moderately humid climate. The incision at 3.3 ± 0.2 ka in the present study is matched with the palaeoflood events in the Ghaggar–Hakra plain of Punjab around 3.9 ka (Singh *et al.* 2021). Our geochemical data of the exposed section is very much similar to the one of the drill core data from Singh *et al.* (2016) and confirms the existence of a large river.

6. Conclusions

This palaeochannel implies that the river which brought the sediments is reworked and mostly from Siwaliks. It can be correlated as the sediments are reworked and matured, derived from the recycled orogenic terrain like granite-gneisses or quartz sedimentary provenance. Hence, the sediments that this river has brought may have faced cycles of transportation. The alternate occurrence of silty clay beds with sand beds indicates a change in the climatic condition. Tectonic setting, provenance, and source area weathering of these sediments clearly show that sediments are from Higher Himalayas and Siwaliks, and are influenced by the change in the climatic conditions.

Author statement

Tarasha Chitkara has carried out the grain size analysis, heavy mineral analysis and geochemical analysis. She also contributed in the interpretation of the data and drafting of the manuscript with the help of Anupam Sharma. Geochemical interpretation was done by Anupam Sharma. O P Thakur and N N Dogra contributed to concluding and framing the paper.

References

Adamiec G and Aitken M J 1998 Dose-rate conversion factors: Update; *Anc. TL* **16** 37–50.

Aitken M J 1998 *Introduction to optical dating: The dating of quaternary sediments by the use of photon-stimulated luminescence*; Clarendon Press.

Basu A 1985 Influence of climate and relief on compositions of sands released at source areas; *Provenance of Arenites*, pp. 1–18, https://doi.org/10.1007/978-94-017-2809-6_1.

Baud A, Atudorei V and Sharp Z 1996 Late Permian and Early Triassic evolution of the Northern Indian margin: Carbon isotope and sequence stratigraphy; *Geodinamica Acta* **9(2–3)** 57–77, https://doi.org/10.1080/09853111.1996.11105278.

Bauluz B, Mayayo M J, Fernandez-Nieto C and Lopez J M G 2000 Geochemistry of Precambrian and Paleozoic siliciclastic rocks from the Iberian Range (NE Spain): Implications for source-area weathering, sorting, provenance, and tectonic setting; *Chem. Geol.* **168(1–2)** 135–150, https://doi.org/10.1016/S0009-2541(00)00192-3.

Bhatia M R 1983 Plate tectonics and geochemical composition of sandstones; *J. Geol.* **91** 611–627, https://doi.org/10.1086/628815.

Bhatia M R 1984 Composition and classification of Paleozoic flysch mudrocks of eastern Australia: Implications in provenance and tectonic setting interpretation; *Sedim. Geol.* **41** 249–268, https://doi.org/10.1016/0037-0738(84)90065-4.

Bhatia M R 1985 Rare-earth elements geochemistry of Australian Paleozoic Graywackes and mud rocks, provenance and tectonic control; *Sedim. Geol.* **45** 97–113, https://doi.org/10.1016/0037-0738(85)90025-9.

Bhatia M R and Crook K A 1986 Trace element characteristics of graywackes and tectonic setting discrimination of sedimentary basins; *Contrib. Mineral. Petrol.* **92(2)** 181–193, https://doi.org/10.1007/BF00375292.

Bøtter-Jensen L, Thomsen K J and Jain M 2010 Review of optically stimulated luminescence (OSL) instrumental developments for retrospective dosimetry; *Radiat. Meas.* **45** 253–257.

Carroll D 1953 Weatherability of zircon; *J. Sedim. Res.* **23** 106–116, https://doi.org/10.1306/D4269562-2B26-11D7-8648000102C1865D.

Chaudhari A R 2021 Saraswati River in northern India (Haryana) and its role in populating the Harappan civilisation sites – A study based on remote sensing, sedimentology, and strata chronology; *Archeological Prospection* **28** 4, https://doi.org/10.1002/arp.1829.

Chauhan M S, Pokharia A K and Srivastava R K 2015 Late Quaternary vegetation history climatic variability and human activity in the Central Ganga Plain deduced by pollen proxy records from Karela Jheel India; *Quat. Int.* **371** 144–156.

Cleary W J and Conolly J R 1972 Embayed quartz grains in soils and their significance; *J. Sedim. Petrol.* **42** 899–904, https://doi.org/10.1306/74D7266C-2B21-11D7-8648000102C1865D.

Colin F, Alarcon C and Vieillard P 1993 Zircon: An immobile index in soils?; *Chem. Geol.* **107** 273–276.

Condie K C, Boryta M D, Liu J and Qian X 1992 The origin of Khondalites: Geochemical evidence from the Archean to Early Proterozoic granulite belt in the North China craton; *Precamb. Res.* **59** 207–223, https://doi.org/10.1016/0301-9268(92)90057-U.

Cordier S, Frechen M and Tsukamoto S 2010 Methodological aspects on luminescence dating of fluvial sands from the moselle basin Luxembourg; *Geochronometria* **35** 67–74, https://doi.org/10.2478/v10003-010-0006-4.

Crook K A 1968 Weathering and roundness of quartz sand grains; *Sedimentology* **11(3–4)** 171–182, https://doi.org/10.1111/j.1365-3091.1968.tb00851.x.

Cullers R L, Basu A and Suttner L J 1988 Geochemical signature of provenance in sand-size material in soils and stream sediments near the Tobacco Root batholith, Montana, USA; *Chem. Geol.* **70(4)** 335–348.

Dabard M P 1990 Lower Brioverian formations (Upper Proterozoic) of the Armorican Massif (France): Geodynamic evolution of source areas revealed by sandstone petrography and geochemistry; *Sedim. Geol.* **69** 45–58, https://doi.org/10.1016/0037-0738(90)90100-8.

Duller G A T 1996 Recent developments in luminescence dating of Quaternary sediments; *Prog. Phys. Geogr.* **20** 127–145.

Fedo C M, Wayne Nesbitt H and Young G M 1995 Unravelling the effects of potassium metasomatism in sedimentary rocks and paleosols, with implications for paleoweathering conditions and provenance; *Geology* **23(10)** 921–924.

Fedo C M, Eriksson K A and Krogstad E J 1996 Geochemistry of shales from the Archean (∼3.0 Ga) Buhwa Greenstone Belt, Zimbabwe: Implications for provenance and source-area weathering; *Geochim. Cosmochim. Acta* **60(10)** 1751–1763.

Feng R and Kerrich R 1990 Geobarometry, differential block movements, and crustal, structure of the southwestern Abitibi greenstone belt, Canada; *Geology* **18(9)** 870–873.

Fralick P W and Kronberg B I 1997 Geochemical discrimination of clastic sedimentary rock sources; *Sedim. Geol.* **113(1–2)** 111–124.

Franzini M, Leoni L and Saitta M 1972 A simple method to evaluate the matrix effects in X-Ray fluorescence analysis; *X Ray Spectrom.* **1** 151–154, https://doi.org/10.1002/xrs.1300010406.

Garver J I and Scott T J 1995 Trace elements in shale as indicators of crustal provenance and terrain accretion in south Canadian Cordillera; *Geol. Soc. Am. Bull.* **107** 440–453, https://doi.org/10.1130/0016-7606(1995)107<0440:TEISAI>2.3.CO;2.

Götze J and Lewis R 1994 Distribution of REE and trace elements in size and mineral fractions of high-purity quartz sands; *Chem. Geol.* **114** 43–57, https://doi.org/10.1016/0009-2541(94)90040-X.

Herron M M 1988 Geochemical classification of terrigenous sands and shales from core or log data; *J. Sedim. Petrol.* **58** 820–829, https://doi.org/10.1306/212F8E77-2B24-11D7-8648000102C1865D.

Hester N C 1974 Post-depositional subaerial weathering effects on the mineralogy of an Upper Cretaceous sand in southeastern United States; *J. Sedim. Res.* **44(2)** 363–373, https://doi.org/10.1306/74D72A31-2B21-11D7-8648000102C1865D.

Horbe A M C, Horbe M A and Suguio K 2004 Tropical spodosols in northeastern Amazonas State, Brazil; *Geoderma* **119** 55–68, https://doi.org/10.1002/arp.1829.

Hubert J F 1962 A zircon-tourmaline-rutile maturity index and the interdependence of the composition of heavy mineral assemblages with the gross composition and texture of sandstones; *J. Sedim. Res.* **32(3)** 440–450.

Jackson M L 1956 Soil chemical analysis – advanced course; Dept. of Soils, Univ. Wisconsin, Madison.

Jain M, Tandon S K and Bhatt S C 2004 Late Quaternary stratigraphic development in the lower Luni Mahi and Sabarmati river basins western India; *Proc. Indian Acad. Sci. (Earth Planet. Sci.)* **113** 453–471, https://doi.org/10.1007/BF02716736.

Keller W D 1962 Diagenesis in clay minerals – a review; *Clays and Clay Minerals* **11(1)** 136–157, https://doi.org/10.1346/CCMN.1962.0110113.

Keller W D 1970a Environmental aspects of clay minerals; *J. Sedim. Res.* **40(3)**, https://doi.org/10.1306/74D720A4-2B21-11D7-8648000102C1865D.

Keller W D 1970b Environmental aspects of clay minerals; *J. Sedim. Res.* **40(3)** 788–813.

Kunze G W and Dixon J 1986 Pretreatment for mineralogical analysis. Methods soil analalysis, Part 1; *Phys. Mineral. Methods* **5** 91–100.

Li C and Yang S Y 2010 Is chemical index of alteration a reliable proxy for chemical weathering in global drainage basins?; *Am. J. Sci.* **310** 111–127, https://doi.org/10.2475/02.2010.03.

Madhavaraju J, Ramírez-Montoya E, Monreal R, González-León C M, Pi-Puig T, Espinoza-Maldonado I G and Grijalva-Noriega F J 2016 Paleoclimate, paleoweathering and paleoredox conditions of Lower Cretaceous shales from the Mural Limestone, Tuape section, northern Sonora, Mexico: Constraints from clay mineralogy and geochemistry; *Revista Mexicana de Ciencias Geológicas* **33(1)** 34–48.

Maynard J B, Valloni R and Yu H S 1982 Composition of modern deep-sea sands arc related basins; In: Trench forearc geology: Sedimentation and tectonics on modern and ancient active plate margin (ed.) Leggett J K, *Geol. Soc. London, Spec. Publ.* **10** 551–561.

McCann T 1998 Sandstone composition and provenance of the Rotliegend of the NE German Basin; *Sedim. Geol.* **116(3–4)** 177–198.

McDonough W F and Sun S S 1995 The composition of the Earth; *Chem. Geol.* **120(3–4)** 223–253.

McLennan S M and Taylor J R 1991 Sedimentary rocks and crustal evolution: Tectonic setting and secular trends; *J. Geol.* **99** 1–21, https://doi.org/10.1086/629470.

McLennan S M, Nance W B and Taylor W B 1980 Rare-earth element-thorium correlations in sedimentary rocks, and the composition of the continental crust; *Geochim. Cosmochim. Acta* **44** 1833–1839, https://doi.org/10.1016/0016-7037(80)90232-X.

McLennan S M, Hemming S, McDaniel D K and Hanson G N 1993 Geochemical approaches to sedimentation, provenance and tectonics; In: Processes controlling the

composition of clastic sediments (eds) Johnsson M J and Basu A, *Geol. Soc. Am. Spec. Paper* **284** 21–40, https://doi.org/10.1130/SPE284-p21.

McLennan S M, Bock B, Compston W, Hemming S R and McDaniel D K 2001 Detrital zircon geochronology of Taconian and Acadian foreland sedimentary rocks in New England; *J. Sedim. Res.* **71(2)** 305–317, https://doi.org/10.1306/072600710305.

Middelburg J J, Van Der Weijden C H and Woittiez J R W 1988 Chemical processes affecting the mobility of major, minor and trace elements during weathering of granitic rocks; *Chem. Geol.* **68** 253–273, https://doi.org/10.1016/0009-2541(88)90025-3.

Morthekai P and Ali S N 2014 Luminescence dating using quartz – for end-users; *Gondwana Geol. Mag.* **29** 1–10.

Morton A C 1985a A new approach to provenance studies: Electron microprobe analysis of detrital garnets from Middle Jurassic sandstones of the northern North Sea; *Sedimentology* **32(4)** 553–566.

Morton J P 1985b Rb–Sr evidence for punctuated illite/smectite diagenesis in the Oligocene Frio Formation, Texas Gulf Coast; *Geol. Soc. Am. Bull.* **96** 114–122, https://doi.org/10.1130/0016-7606(1985)96<114:REFPID>2.0.CO;2.

Myrow P M, Hughes N C, Derry L A, McKenzie N R, Jiang G, Webb A A G, Banerjee D M, Paulsen T S and Singh B S 2015 Neogene marine isotopic evolution and the erosion of Lsser Himalayan strata: Implications for Cenozoic tectonic history; *Earth Planet. Sci. Lett.* **417** 142–150.

Nagarajan R, Armstrong-Altrin J S, Nagendra R, Madhavaraju J and Moutte J 2007a Petrography and geochemistry of terrigenous sedimentary rocks in the Neo-proterozoic Rabanpalli Formation, Bhima Basin, southern India: Implications for paleoweathering condition, provenance, and source rock composition; *J. Geol. Soc. India* **70** 297–312.

Nagarajan R, Madhavaraju J, Nagendra R, Armstrong-Altrin J S and Moutte J 2007b Geochemistry of Neoproterozoic shales of Rabanpalli Formation, Bhima Basin, northern Karnataka, southern India: Implications for provenance and paleoredox conditions; *Revista Mexicana de Ciencias Geologicas* **24** 150–160, https://hal-emse.ccsd.cnrs.fr/emse-00612104.

Nesbitt H W and Young G M 1982 Early proterozoic climates and plate motions inferred from major element chemistry of lutites; *Nature* **299** 715–717, https://doi.org/10.1038/299715a0.

Nesbitt H W and Young G M 1984 Prediction of some weathering trends of plutonic and volcanic rocks based on thermodynamic and kinetic considerations; *Geochim; Cosmochim. Acta* **48** 1523–1534, https://doi.org/10.1016/0016-7037(84)90408-3.

Nesbitt H W and Young G M 1989 Formation and diagenesis of weathering profiles; *J. Geol.* **97** 129–147, https://www.jstor.org/stable/30065535.

Nesbitt H W, Young G M, McLennan S M and Keays R R 1996 Effects of chemical weathering and sorting on the petrogenesis of siliciclastic sediments, with implications for provenance studies; *J. Geol.* **104(5)** 525–542.

Oliva P, Viers J, Dupré B, Fortuné J P, Martin F, Braun J J, Nahon D and Robain H 1999 The effect of organic matter on chemical weathering: Study of a small tropical watershed: Nsimi-Zoetele site, Cameroon; *Geochim. Cosmochim. Acta* **63(23–24)** 4013–4035, https://doi.org/10.1016/S0016-7037(99)00306-3.

Pettijohn F J 1972 The Archean of the Canadian shield: A resume; https://doi.org/10.1130/MEM135-p131.

Pettijohn F J, Potter P E and Siever R 1972 *Sand and sandstone*; Springer-Verlag, New York, 618p.

Pettijohn F J, Potter P E and Siever R 1973 *Sand and sandstones*; Springer Verlag, New York; https://doi.org/10.1007/978-1-4615-9974-6.

Prescott J R and Hutton J T 1994 Cosmic ray contributions to dose rates for luminescence and ESR dating: Large depths and long-term time variations; *Radiat. Meas.* **23** 497–500.

Richards A, Argles T, Harris N, Parrish R, Ahmad T, Darbyshire F and Draganits E 2005 Himalayan architecture constrained by isotopic tracers from clastic sediments; *Earth Planet. Sci. Lett.* **236(3–4)** 773–796, https://doi.org/10.1016/j.epsl.2005.05.034.

Roscher B P and Korsch R J 1986 Determination of tectonic setting of sandstone-mudstone suites using SiO_2 content and K_2O/Na_2O ratio; *J. Geol.* **94** 635–650, https://doi.org/10.1086/629071.

Roser B P and Korsch R J 1988 Provenance signatures of sandstone-mudstone suites determined using discriminant function analysis of major-element data; *Chem. Geol.* **67** 119–139, https://doi.org/10.1016/0009-2541(88)90010-1.

Rudnick R L and Gao S 2003 Composition of the continental crust; *Treatise on Geochemistry*, pp. 1–64, **ISBN (set): 0-08-043751-6, 3 (ISBN: 0-08-0044338-9)**.

Saxena A, Trivedi A, Chauhan M S and Sharma A 2015 Holocene vegetation and climate change in Central Ganga Plain: A study based on multiproxy records from Chaudhary-Ka-Tal Raebareli District, Uttar Pradesh, India; *Quat. Int.* **371** 164–174.

Sharma S, Joachimski M M, Tobschall H J, Singh I B, Sharma C and Chauhan M S 2004 Correlative evidences of monsoon variability, vegetation change and human inhabitation in Sanai Lake deposit: Ganga Plain, India; *Curr. Sci.* **90** 973–978.

Singh I B 1996 Geological evolution of Ganga Plain – An overview; *J. Palaeontol. Soc. India* **41** 99–137.

Singh P 2009 Major, trace and REE geochemistry of the Ganga River sediments: Influence of provenance and sedimentary processes; *Chem. Geol.* **266(3–4)** 242–255, https://doi.org/10.1016/j.chemgeo.2009.06.013.

Singh P 2010 Geochemistry and provenance of stream sediments of the Ganga River and its major tributaries in the Himalayan region, India; *Chem. Geol.* **269(3–4)** 220–236.

Singh P and Rajamani V 2001a Geochemistry of the Kaveri flood plain sediments, southern India; *J. Sedim. Res.* **711** 50–60.

Singh P and Rajamani V 2001b REE Geochemistry of recent clastic sediments from the Kaveri floodplains, southern India: Implication to source area weathering and sedimentary processes; *Geochim. Cosmochim. Acta* **65** 3093–3108.

Singh A and Sinha R 2019 Fluvial response to climate change inferred from sediment cores from the Ghaggar–Hakra paleochannel in NW Indo–Gangetic plains; *Palaeogeogr. Palaeoclimatol. Palaeoecol.* **532** 109247.

Singh I B, Rajagopalan G, Agarwal K K, Srivastava P, Sharma M and Sharma S 1997 Evidence of Middle to Late Holocene neotectonic activity in the Ganga Plain; *Curr. Sci.* **73(12)** 1114–1117.

Singh A, Paul D, Sinha R, Thomsen K J and Gupta S 2016 Geochemistry of buried river sediments from Ghaggar Plains, NW India: Multi-proxy records of variations in provenance,

paleoclimate, and paleovegetation patterns in the Late Quaternary; *Palaeogeogr. Palaeoclimatol. Palaeoecol.* **449** 85–100, https://doi.org/10.1016/j.paleo.2016.02.012.

Singh A, Jain V, Danino M, Chauhan N, Kaushal R K, Guha S and Prabhakar V N 2021 Larger floods of Himalayan foothill rivers sustained flows in the Ghaggar–Hakra channel during Harappan age; *J. Quat. Sci.* **36(4)** 611–627, https://doi.org/10.1002/jqs.3320.

Sinha S, Islam R, Ghosh S K, Kumar R and Sangode S J 2007 Geochemistry of Neogene Siwalik mudstones along Punjab re-entrant, India: Implications for source-area weathering, provenance and tectonic setting; *Curr. Sci.* **92(8)** 1103–1113, http://www.jstor.org/stable/24097629.

Sinha R, Yadav G S, Gupta S, Singh A and Lahiri S K 2013 Geoelectric resistivity evidence for subsurface paleochannel systems adjacent to Harappan sites in northwest India; *Quat. Int.* **308** 66–75, https://doi.org/10.1016/j.quaint.2012.08.002.

Tang Y, Sang L, Yuan Y, Zhang Y and Yang Y 2012 Geochemistry of Late Triassic pelitic rocks in the NE part of Songpan-Ganzi Basin, western China: Implications for source weathering, provenance and tectonic setting; *Geosci. Frontiers* **3(5)** 647–660, https://doi.org/10.1016/j.gsf.2012.01.006.

Taylor S R and McLennan S M 1981 The composition and evolution of the continental crust: Rare earth element evidence from sedimentary rocks; *Philos.* **A301** 381–399, https://doi.org/10.1098/rsta.1981.0119.

Taylor S R and McLennan S M 1983 Geochemistry of early Proterozoic sedimentary rocks and the Archean/Proterozoic boundary; *Proterozoic geology: Selected papers from an international Proterozoic symposium: Geol. Soc. Am., Memoir* **161** 119–131.

Taylor S R and McLennan S M 1985 *The continental crust: Its composition and evolution*; Blackwell Publishers, 312p.

Thomas M, Thorp M and McAlister J 1999 Equatorial weathering, landform development and the formation of white sands in northwestern Kalimantan, Indonesia; *Catena* **36** 205–232, https://doi.org/10.1016/S0341-8162(99)00014-4.

Thussu J L 1995 Quaternary stratigraphy and sedimentation of the Indo-Gangetic plains, Haryana; *J. Geol. Soc. India* **46(5)** 533–543.

Tripathi J K and Rajamani V 2003 Geochemistry of Proterozoic Delhi quartzites: Implications for the provenance and source area weathering; *Geol. Soc. India* **62(2)** 215–226.

Tripathi J K, Bock B, Rajamani V and Eisenhauer J 2004 Is river Ghaggar, Saraswati? Geochemical constraints; *Curr. Sci.* **87** 1141–1145, http://doi.org/0011-3891.

Trivedi A, Chauhan M S, Sharma A, Nautiyal C M and Tiwari D P 2013 Record of vegetation and climate during Late Pleistocene–Holocene in Central Ganga Plain based on multiproxy data from Jalesar Lake Uttar Pradesh India; *Quat. Int.* **306** 97–106.

Valdiya K S 2003 Reactivation of Himalayan frontal fault: Implications; *Curr. Sci.* **85(7)** 1031–1040.

Valdiya K S 2005 Trans Himadari Fault: Tectonics of detachment system in Central Sector of Himalaya, India; *J. Geol. Soc. India* **1–2** 53–63.

Valdiya K S 2013 The River Saraswati was a Himalayan-born river; *Curr. Sci.* **104** 42–54.

Valdiya K S 2015 *The making of India: Geodynamic evolution*; Springer.

Valdiya K S 2016 *Prehistoric river Saraswati: Geological appraisal and social aspects*; Springer, 136p.

Van Loon A J and Mange A M 2007 "In situ" dissolution of heavy minerals through extreme weathering, and the application of the surviving assemblages and their dissolution characteristics to correlation of Dutch and German silver sands; *Dev. Sedimentol. Ser.* **58** 189–213, https://doi.org/10.1016/S0070-4571(07)58006-4.

Vannay J-C, Grasemann B, Rahn M, Frank W, Carter A, Baudraz V and Cosca M 2004 Miocene to Holocene exhumation of metamorphic crustal wedges in the NW Himalaya: Evidence for tectonic extrusion coupled to fluvial erosion; *Tectonics* **23(1)** 1–24.

Vital H, Stattegger K and Garbe-Schoenberg C D 1999 Composition and trace-element geochemistry of detrital clay and heavy-mineral suites of the lowermost Amazon River: A provenance study; *J. Sedim. Res.* **69(3)** 563–575, https://doi.org/10.2110/jsr.69.563.

Wallinga J 2002 Optically stimulated luminescence dating of fluvial deposits: A review; *Boreas* **31** 303–322.

Webb A A G, Yin A, Harrison T M, Célérier J, Gehrels G E, Manning C E and Grove M 2011 Cenozoic tectonic history of the Himachal Himalaya (northwestern India) and its constraints on the formation mechanism of the Himalayan orogen; *Geosphere* **7(4)** 1013–1061.

Whitmore G P, Crook K A W and Johnson D 2004 Grain size control of mineralogy and geochemistry in modern river sediment, New Guinea collision, Papua New Guinea; *Sedim. Geol.* **171** 129–157, https://doi.org/10.1016/j.sedgeo.2004.03.011.

Wronkiewicz D J and Condie K C 1987 Geochemistry of Archean shales from the Witwatersrand Supergroup, South Africa: Source-area weathering and provenance; *Geochim. Cosmochim. Acta* **51(9)** 2401–2416, https://doi.org/10.1016/0016-7037(87)90293-6.

Wyborn L A and Chappell B W 1983 Chemistry of the Ordovician and Silurian greywackes of the Snowy Mountains, southeastern Australia: An example of chemical evolution of sediments with time; *Chem. Geol.* **39(1–2)** 81–92, https://doi.org/10.1016/0009-2541(83)90073-6.

Yashpal S B, Sood R K and Agrawal D P 1980 Remote sensing of the 'lost' Saraswati' river; *Proc. Indian Acad. Sci. (Earth Planet Sci.)* **89** 317–331.

Yin A 2006 Cenozoic tectonic evolution of the Himalayan orogen as constrained by along-strike variation of structural geometry, exhumation history, and foreland sedimentation; *Earth-Sci. Rev.* **76(1–2)** 1–131.

Corresponding editor: George Mathew